Naval Research Laboratory
Washington, DC 20375-5000

NRL Memorandum Report 6331

Evaluation and Additional Documentation of the Parabolic Marching Code Surfwake

E. WADE MINER AND THOMAS F. SWEAN, JR.

Center for Hydrodynamic Developments
Laboratory for Computational Physics and Fluid Dynamics

ARMIN TROESCH

Department of Naval Architecture
and Marine Engineering
University of Michigan

September 22, 1988

SECURITY CLASSIFICATION OF THIS PAGE

REPORT DOCUMENTATION PAGE

Form Approved
OMB No 0704-0188

1a. REPORT SECURITY CLASSIFICATION UNCLASSIFIED	1b RESTRICTIVE MARKINGS
2a. SECURITY CLASSIFICATION AUTHORITY	3 DISTRIBUTION / AVAILABILITY OF REPORT Approved for public release; distribution unlimited.
2b. DECLASSIFICATION / DOWNGRADING SCHEDULE	
4. PERFORMING ORGANIZATION REPORT NUMBER(S) NRL Memorandum Report 6331	5 MONITORING ORGANIZATION REPORT NUMBER(S)
6a. NAME OF PERFORMING ORGANIZATION Naval Research Laboratory 6b OFFICE SYMBOL (If applicable) Code 4430	7a. NAME OF MONITORING ORGANIZATION
6c. ADDRESS (City, State, and ZIP Code) Washington, DC 20375-5000	7b ADDRESS (City, State, and ZIP Code)
8a. NAME OF FUNDING / SPONSORING ORGANIZATION Office of Naval Research 8b. OFFICE SYMBOL (If applicable)	9 PROCUREMENT INSTRUMENT IDENTIFICATION NUMBER
8c. ADDRESS (City, State, and ZIP Code) Arlington, VA 22217	10 SOURCE OF FUNDING NUMBERS PROGRAM ELEMENT NO: 61153N; PROJECT NO:; TASK NO: RR023-01-00; WORK UNIT ACCESSION NO: DN157-111

11. TITLE (Include Security Classification)
Evaluation and Additional Documentation of the Parabolic Marching Code Surfwake

12. PERSONAL AUTHOR(S)
Miner, E.W., Troesch, A. and Swean, T.F., Jr.

13a. TYPE OF REPORT	13b TIME COVERED	14 DATE OF REPORT (Year, Month, Day)	15 PAGE COUNT
Interim	FROM 1/88 TO 6/88	1988 September 22	57

16. SUPPLEMENTARY NOTATION

17 COSATI CODES		
FIELD	GROUP	SUB-GROUP

18 SUBJECT TERMS (Continue on reverse if necessary and identify by block number)
Turbulent ship wake, Finite difference calculations
Self propelled wake, SURFWAKE programmer's manual

19 ABSTRACT (Continue on reverse if necessary and identify by block number)

The capabilities of the parabolic marching code SURFWAKE for simulating the turbulent wake of a surface ship are evaluated for one set of experimental conditions. For the conditions considered, it is determined that the results from the code agree well with the results previously obtained with the NRL code TWAKE when the "rigid-lid" approximation to the free surface is used. When the linearized free surface boundary condition is used, the code gives poor simulations for the transverse velocities. Additional capabilities are added to the program and documented. The new capabilities permit the user greater flexibility in providing the input data required to initialize a turbulent wake simulation. For the conditions considered, the SURFWAKE code requires less computer time for the simulations than does the TWAKE code. The code has been executed for the given data on Hewlett-Packard and Digital Equipment computer systems with identical results to 4 significant figures for single precision compliations.

20 DISTRIBUTION / AVAILABILITY OF ABSTRACT ☒ UNCLASSIFIED/UNLIMITED ☐ SAME AS RPT ☐ DTIC USERS	21 ABSTRACT SECURITY CLASSIFICATION UNCLASSIFIED
22a NAME OF RESPONSIBLE INDIVIDUAL E. Wade Miner	22b TELEPHONE (Include Area Code) 22c OFFICE SYMBOL (202) 767-3368 Code 4430

DD Form 1473, JUN 86 Previous editions are obsolete

S/N 0102-LF-014-6603

CONTENTS

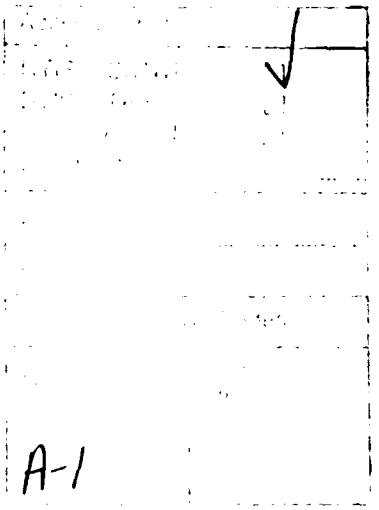

EVALUATION AND ADDITIONAL DOCUMENTATION OF THE PARABOLIC MARCHING CODE SURFWAKE

1. INTRODUCTION

In a recent report, Swean (Ref. [1]) presented results which were obtained from the numerical simulations of the wake of a high speed surface ship. Those numerical simulations were for conditions matching a series of experiments which have been conducted at the David Taylor Research Center (DTRC) for the surface wake of a self-propelled model of a twin-screw destroyer. The initial conditions for the calculations were generated from the experimental data that had been made available to the Naval Research Laboratory (NRL). Those calculations were performed with the NRL code TWAKE.

Recently, the Ship Wake Consortium has been formed by the Office of Naval Research (ONR) combining the cooperative efforts of the University of Michigan, DTRC and NRL. As a part of the research work of the consortium, the code SURFWAKE has been made available to NRL for evaluation and documentation. The SURFWAKE code has several apparent advantages compared to the TWAKE code used by Swean (Ref. [1]). In the TWAKE code, the available free surface boundary condition is the "rigid-lid" approximation. SURFWAKE includes provisions for both the "rigid-lid" boundary condition and a linearized free surface boundary condition. SURFWAKE also includes the capability for simulations of stratified flow fields. Further, SURFWAKE has the potential to be easier and more economical to use than TWAKE. On the basis of these potentially attractive characteristics, it is desirable to evaluate the capabilities of the computer program.

Unfortunately, the version of SURFWAKE retained by the Consortium is not fully documented and for this reason has not been used within Navy programs until this time. The deficiencies in documentation have to do with how to properly initiate a computation with arbitrary, perhaps experimentally derived, initial conditions, and the nature of the options regarding the free surface boundary conditions. Refs. [2-4] provide fairly extensive documentation of the program FASTWAKE, a well-known computer program within the Navy community. SURFWAKE is a derivative of this computer program and is described to an extent in Ref. [5]. That report, however, does not contain documentation of the changes to the original computer program which would be useful to the programmer or user.

The purpose of this report is three-fold: the first is to provide the additional necessary documentation for initializing a surface ship wake computation, the second

Manuscript approved June 29, 1988.

is to evaluate the capabilities of SURFWAKE to simulate the turbulent wake of a surface ship, and the third is to expose the nature of the available linearized free surface boundary condition option and to determine its effects in a typical computation. The first of these is rather easily disposed of and that material is included in Appendix A. That material stands alone from the remainder of this report and the reader who is interested only in executing the computer program for a given fluid initial condition may proceed directly to Appendix A. A familiarity with the original FASTWAKE user's manual (Ref. [2]) is, however, assumed.

During the course of pursuing the second and third objectives above, some minor programming errors were uncovered. These errors and the steps to correct them will be documented as appropriate in subsequent sections of this report. The evaluation of the program's ability to accurately simulate turbulent ship wakes is less easily accomplished due to the lack of documented experimental data. The computations of Ref. [1], however, are at least in qualitive agreement with preliminary but unpublished experimental data (Refs. [6,7]) and for that reason, this report will discuss an attempt to compute the same flow. Two different free surface boundary conditions were employed during the computations; the first was the familiar "rigid-lid" boundary condition used by nearly all computations of this type (and in Ref. [1]), and the second was the linearized free surface boundary condition proposed by Meng, et al. [5]. Contrasting the results of these separate computations and with those of Swean [1] provides the means to accomplish the second and third objectives.

The next section will give a brief overview of the computational model used in SURFWAKE. Included will be a discussion of the free surface boundary conditions. Where appropriate, attention will be drawn to the differences between this code and the TWAKE code referenced above. The final section will present the results of the two calculations and contrast them amongst each other and with those of Ref. [1].

2. DESCRIPTION OF THE SURFWAKE COMPUTATIONAL MODEL

The SURFWAKE code is a derivative of the FASTWAKE code developed by Meng and Innis and documented in Ref. [2]. The turbulence model which was used in that version of FASTWAKE used transport equations for the turbulence kinetic energy and the enstrophy which is the square of the turbulence vorticity. The turbulence model was subsequently modified (Refs. [3,4]) to use transport equations for the turbulence kinetic energy and the dissipation function, ϵ. The governing equation set used in FASTWAKE is similar to the equation set used in TWAKE. The SURFWAKE code was derived from FASTWAKE by Meng (Ref. [5]) by the addition of boundary conditions suitable for a free surface.

The transport equations solved by SURFWAKE are the Reynolds-averaged, steady, parabolic Navier-Stokes equations. The flow field variables are separated into a non-zero ensemble mean part and a zero-mean fluctuating part. The mean field is further written as a sum of an ambient field term and the departure from that field due to the wake. The spatial coordinate system is fixed in the body so that the ambient flow has a constant axial component U_0 along the x-axis. The z-axis is positive upward and the y-axis is defined by the right-hand-rule. Thus the velocity and density fields are :

$$\begin{aligned} U(x,y,z) &= U_0 + u(x,y,z) + u'(x,y,z) \\ V(x,y,z) &= V_0(z) + v(x,y,z) + v'(x,y,z) \\ W(x,y,z) &= w(x,y,z) + w'(x,y,z) \\ \varrho(x,y,z) &= \rho_0(z) + \rho(x,y,z) + \rho'(x,y,z) \end{aligned}$$

The formulation allows for an ambient flow with a transverse component $V_0(z)$. With this velocity and density decomposition, the ensemble-averaged parabolic Navier-Stokes equations as solved by SURFWAKE are:

continuity:

$$\frac{\partial u}{\partial x} + \frac{\partial v}{\partial y} + \frac{\partial w}{\partial z} = 0, \tag{1}$$

axial momentum:

$$U_0 \frac{\partial u}{\partial x} + \frac{\partial uv}{\partial y} + \frac{\partial uw}{\partial z} = \nu\left(\frac{\partial^2 u}{\partial y^2} + \frac{\partial^2 u}{\partial z^2}\right) - \frac{\partial(\overline{u'v'})}{\partial y} - \frac{\partial(\overline{u'w'})}{\partial z}. \tag{2}$$

vertical momentum:

$$\frac{\partial(U_0+u)w}{\partial x} + \frac{\partial vw}{\partial y} + \frac{\partial ww}{\partial z} = -\frac{1}{\rho_0}\frac{\partial p}{\partial z} + \nu\left(\frac{\partial^2 w}{\partial y^2} + \frac{\partial^2 w}{\partial z^2}\right) - g\frac{\rho}{\rho_0} - \frac{\partial(\overline{v'w'})}{\partial y} - \frac{\partial(\overline{w'w'})}{\partial z}. \tag{3}$$

transverse momentum:

$$\frac{\partial(U_0+u)v}{\partial x} + \frac{\partial vv}{\partial y} + \frac{\partial vw}{\partial z} = -\frac{1}{\rho_0}\frac{\partial p}{\partial y} + \nu\left(\frac{\partial^2 v}{\partial y^2} + \frac{\partial^2 v}{\partial z^2}\right) - \frac{\partial(\overline{v'v'})}{\partial y} - \frac{\partial(\overline{v'w'})}{\partial z}. \tag{4}$$

The turbulence velocity and density correlations in the above equations are computed from the set of algebraic relations:

$$\overline{u_i' u_j'} = \frac{2}{3}\delta_{ij}\, q + C_2 \frac{q}{\epsilon}\Big(\mathcal{P}_{ij} + \mathcal{G}_{ij} - \frac{2}{3}\delta_{ij}(\mathcal{P} + \mathcal{G})\Big) + C_1 C_2 \frac{q^2}{\epsilon}\mathcal{S}_{ij}, \tag{5}$$

$$\overline{\rho' u_i'} = -C_{\rho 1}\, \frac{q}{\epsilon}\Big(\overline{u_i' u_j'}\, \frac{\partial \rho}{\partial x_j} + \overline{\rho' u_j'}\, \frac{\partial u_i}{\partial x_j} - \frac{g_i}{\rho_0}\, \overline{\rho' \rho'}\Big), \tag{6}$$

$$\overline{\rho' \rho'} = -C_{\rho 2}\, \frac{q}{\epsilon}\, \overline{\rho' u_i'}\, \frac{\partial \rho}{\partial x_i}, \tag{7}$$

where:

$$\mathcal{P}_{ij} \equiv -\overline{u_i' u_k'}\, \frac{\partial u_j}{\partial x_k} - \overline{u_j' u_k'}\, \frac{\partial u_i}{\partial x_k}, \tag{8}$$

$$\mathcal{G}_{ij} \equiv \frac{g_i}{\rho_0}\, \overline{\rho' u_j'} + \frac{g_j}{\rho_0}\, \overline{\rho' u_i'}, \tag{9}$$

$$\mathcal{S}_{ij} \equiv \frac{\partial u_i}{\partial x_j} + \frac{\partial u_j}{\partial x_i}, \tag{10}$$

and where $\mathcal{P} \equiv \frac{1}{2}\mathcal{P}_{kk}$ and $\mathcal{G} \equiv \frac{1}{2}\mathcal{G}_{kk}$ are the production of turbulence kinetic energy by shear and buoyancy, respectively.

The equation set is completed by equations for the density perturbation, ρ, the turbulence kinetic energy, $q \equiv \frac{1}{2}(\overline{u'^2} + \overline{v'^2} + \overline{w'^2})$, and the isotropic dissipation function, ϵ:

density:

$$\frac{\partial (U_0 + u)\rho}{\partial x} + \frac{\partial v \rho}{\partial y} + \frac{\partial w \rho}{\partial z} = -w \frac{\partial \rho_0}{\partial z} - \frac{\partial (\overline{v'\rho'})}{\partial y} - \frac{\partial (\overline{w'\rho'})}{\partial z}. \tag{11}$$

modelled turbulence transport:

$$\frac{\partial (U_0 + u) q}{\partial x} + \frac{\partial v q}{\partial y} + \frac{\partial w q}{\partial z} = \frac{\partial}{\partial y}\Big(C_q \frac{q^2}{\epsilon}\frac{\partial q}{\partial y}\Big) + \frac{\partial}{\partial z}\Big(C_q \frac{q^2}{\epsilon}\frac{\partial q}{\partial z}\Big) + \mathcal{P} - \frac{g}{\rho_0}\overline{w'\rho'} - \epsilon, \tag{12}$$

modelled dissipation function:

$$\frac{\partial (U_0 + u) \epsilon}{\partial x} + \frac{\partial v \epsilon}{\partial y} + \frac{\partial w \epsilon}{\partial z} = \frac{\partial}{\partial y}\Big(C_\epsilon \frac{q^2}{\epsilon}\frac{\partial \epsilon}{\partial y}\Big) + \frac{\partial}{\partial z}\Big(C_\epsilon \frac{q^2}{\epsilon}\frac{\partial \epsilon}{\partial z}\Big) + C_{\epsilon 1}\frac{\epsilon}{q}\mathcal{P} - C_{\epsilon 2}\frac{\epsilon^2}{q}. \tag{13}$$

In this form, the turbulence model contains the eight constants $\{C_1, C_2, C_q, C_\epsilon, C_{\epsilon 1}, C_{\epsilon 2}, C_{\rho 1}, C_{\rho 2}\}$. From Ref. [4], the values of these constants are {0.16, 0.23, 0.15, 0.10, 1.45, 1.80, 0.21, 1.60}. The role of these constants is quite similar to that of the constants used in the turbulence model in TWAKE; however, that model uses four constants in the modelling of the kinematic turbulent stresses and the model in SURFWAKE uses only two. Also, the SURFWAKE model has two density related constants and TWAKE does not solve a density equation.

It should be noted that the ordering analysis used in developing the equation set in SURFWAKE has resulted in the linearization of the axial momentum equation through the omission of the $u\partial u/\partial x$ term. Also note that the cross-shear velocity $V_0(x)$ has been dropped in the above representation of the equation set. The density equation, of course, reduces due to the divergence-free condition on velocity for constant density flows.

The SURFWAKE code requires initial distributions of the three components of mean velocity, the turbulence kinetic energy, and the dissipation function in order to begin a computation. Additionally, SURFWAKE requires an initial distribution of the density. One of the principal objectives of the present work is to compare the results of simulations of the wake flow of the destroyer model obtained with SURFWAKE with the results obtained with TWAKE. In order to make the comparison of results meaningful, the same input initial distributions for the three components of mean velocity and turbulence kinetic energy were used for SURFWAKE as were used for TWAKE with the addition of a constant density distribution.

As described in Ref. [1], the initial distribution for the dissipation function was obtained from the turbulence kinetic energy using Eq. (14) of Ref. [1] and an appropriate scale length l. An analysis was made of the $\overline{u'v'}$ equation in the two turbulence models which suggested that the value of l_d used in SURFWAKE should be approximately 0.55 times that use in TWAKE. This results in $l_d = 0.31\ ft$ rather than $0.58\ ft$ which was used in the calculations in Ref. [1].

In an effort to further insure proper comparability of the results between TWAKE and SURFWAKE , four of the constants in the turbulence model were modified so as to match the constants in TWAKE as nearly as possible. Comparison of Eq. (13) with Eq. (13) in Ref. [1] shows that $C_{\epsilon 1}$ and $C_{\epsilon 2}$ have essentially identical roles in the two models. Thus $C_{\epsilon 1}$ and $C_{\epsilon 2}$ were set to 1.44 and 1.92 respectively. Also, comparison of Eqs. (12 and 13) with Eqs. (12 and 13) in Ref. [1] shows that C_q in Eq. (12) corresponds to C_4/σ_K in Eq. (12) of Ref. [1] and that C_ϵ in Eq. (13) corresponds to C_4/σ_ϵ in Eq. (13) in Ref. [1]. Thus C_q and C_ϵ were set to 0.068 and 0.052 respectively. Clearly some significant differences in the turbulence models still exist and it was not the intent of

the present study to make the two turbulence models the same but it was intended that features which could be easily made comparable should be comparable.

The governing equations in SURFWAKE are solved by an Eulerian finite-difference method. The method is one step explicit and is second order (or better) accurate in the x-direction. The space derivatives are center differenced. The finite-difference method uses a staggered mesh system with the axial velocity excess u, the turbulence kinetic energy q, and the dissipation function ϵ defined on cell centers but the transverse velocities v and w and the density ρ defined on the cell faces. The calculation for the values of the dependent variables at the new time step (or x station) takes place only on the interior points of the grid. The values of the dependent variables on the boundary grid points are determined from the boundary conditions and the variable values at the neighboring grid points. Because the solution procedure uses a staggered mesh grid, the application of the boundary conditions for the transverse velocities and the density are different in form on the right and left sides and on the top and bottom surfaces. The primary boundary conditions are free-slip rigid wall at the four sides.

As noted above, the SURFWAKE code has options for both the "rigid-lid" approximation for the surface boundary condition as well as a linearized free surface boundary condition. Free surface effects were first included in the FASTWAKE code by Meng, et al. [5]. When the free surface option is activated, the various flow variables have to satisfy free surface boundary conditions. The governing equations in the fluid domain and the three-dimensional marching algorithm remain unchanged. Descriptions of the different boundary conditions and their effects on the solution are given below.

The top row of cells in the program SURFWAKE is designated as the free surface. Specifically, the variables are required to satisfy the various free surface boundary conditions on that top row. The number of grid points and y - z coordinates of the grid points are not changed. By not regridding or tracking the exact free surface, the program implies a Taylor series expansion of the upper boundary equations about the mean water surface (i.e. $z = 0$). This modeling is valid for waves with small amplitudes and small slopes but not for steep or near-breaking waves.

The "rigid-lid" approximation is a free-slip rigid wall condition as used at the other three sides of the computation domain. The z-gradients of the horizontal flow velocities, the turbulence kinetic energy, and the dissipation function are set to zero at the boundary and the vertical velocity w is set to zero.

The significant turbulence variables include the Reynolds stresses, the turbulent kinetic energy, and the dissipation function. In addition to the boundary equations

that the variables have to satisfy, there are also closure conditions on the pressure-strain correlation, the pressure-density correlation, and the triple-correlation term in the turbulent kinetic energy rate equation. These equations and closure conditions have the effect of changing the turbulent length scales to reflect the presence of the free surface. For a more detailed justification of the effect of turbulence on the free surface boundary conditions, refer to Meng, et al. [5].

The mean flow variables are also required to satisfy free surface boundary conditions. These are typically expressed as kinematic and dynamic relationships. Given the fixed grid, the problem is effectively linearized with respect to wave amplitude. Also, the relatively large grid spacing precludes the numerical modeling of capillary waves and consequently the effects of surface tension are not considered. In the absence of viscosity this model should, in principle, produce the usual irrotational linear gravity waves.

The modified free surface boundary equations of SURFWAKE are somewhat different than those described by Meng, et al. [5]. The kinematic condition for the free surface elevation,

$$U_0 \frac{\partial \eta}{\partial x} = w \qquad \text{on } z = 0 \tag{14}$$

and the equality between the atmospheric and fluid pressures,

$$P_f = P_a = 0 \qquad \text{on } z = 0 \tag{15}$$

remain unchanged. However, the dynamic condition for stress equilibrium on the surface has been corrected to include the effects of gravity. By assuming that the flow on the surface is inviscid and steady, but not necessarily irrotational, Bernoulli's equation along a streamline can be approximated by

$$U_0 u = -g\eta \qquad \text{on } z = 0 \tag{16}$$

Combining Eqs. (14) and (16) to eliminate the surface elevation, η, the free surface boundary condition for the vertical velocity component, w, becomes

$$U_0^2 \frac{\partial u}{\partial x} + gw = 0 \qquad \text{on } z = 0. \tag{17}$$

The boundary conditions for the horizontal velocity components are approximated as

$$\frac{\partial u}{\partial z} = 0 \quad \text{and} \quad \frac{\partial v}{\partial z} = 0 \quad \text{on } z = 0. \tag{18}$$

SURFWAKE has an option which allows the user to place psuedo wave dampers at one or both of the side boundaries. This option should be activated when free surface modeling is done, otherwise reflected waves may contaminate the results. The user is cautioned, however, that the exact behavior of the dampers has not been determined and example cases should be run for specific applications. Descriptions of the theory and implementation of the dampers are given by Meng and Innis [2] and Chan [8].

3. RESULTS AND DISCUSSION

The evaluation of the SURFWAKE code was accomplished by making numerical simulations for the wake of a ship model for one set of conditions. A series of experiments have been conducted at DTRC to determine the three dimensional turbulent velocity field and the free surface elevations in the wake region of a twin-screw destroyer model. A line drawing of the model is contained in Fig. 1 and Table 1 displays relevant data on the model dimensions and towing conditions.

Table 1. Model Ship Parameters

Model	High Speed Surface Ship
DTRC No.	5415-1
Length*	18.8 *ft*
Beam	29.9 *in*
Draft	9.8 *in*
Prop Dia.	8.16 *in*
Block Coef.	0.506
Tow Speed	4.0 *knots*
Froude No.	0.28

* (length between forward and aft perpendiculars)

Swean [1] used the TWAKE code to simulate the wake for two of the experimental conditions. The experimental conditions are described in Ref. [1] and will be briefly summarized here. Mean velocity and turbulence measurements were taken using both laser doppler velocimetry (LDV) and hot-film annemometry (HF) techniques. The measurement domain consisted of a series of vertical planes at various axial locations in

the wake. A schematic of the model and the coordinate system is shown in Fig. 2a, and a schematic of the typical experimental cross-plane including the major wake producing elements of the model is shown in Fig. 2b. Generally, the sensors were placed at a specified depth (z) and measurements were taken point by point at intervals of 2.0 *in* in the range $-3.0 \leq y \leq 33.0$. The measurement interval in the z direction was also 2.0 *in* from -1.6 *in* (nearest to the free surface) to a maximum depth of between -17.0 *in* to -28.0 *in* depending on the distance aft of the model.

A matrix showing the scope of the measurements obtained is given in Table 2. The numbers in the table refer to the approximate number of points measured for a particular test which is characterized by

1) the distance from the aft perpendicular (AP) to the measurement plane,
2) the tow speed,
3) the rotation direction of the propellers (or unpropelled), and
4) the type of sensor used for the measurements.

The elements denoted by an asterisk have been forwarded to NRL via Refs. [6-7].

Table 2. Points/data planes from LDV and HF anemometry

Feet from AP	-1.7		-1.1		-0.4		6.1		10.0		16.0		22.0		30.0	
Speed, *knots*	4	6	4	6	4	6	4	6	4	6	4	6	4	6	4	6
Outboard, LDV		96		128		111			175*	138	280*†	279†	260*			167
Outboard, LDV												151				
Outboard, HF							70		73*		86*	68	75*		61*	
Inboard, LDV									175*			148				160
No Prop, LDV				117					130			182†				

* (forwarded to NRL)

†(denotes plane where symmetry about vertical plane was tested)

Two of the data sets referenced in Table 2 were used to develop initial conditions for the numerical simulations using TWAKE. These are the 4.0 *knots* data at the 10.0 *ft* plane with both outboard (clockwise) and inboard (counter-clockwise) propeller rotation.

Numerical simulations with the SURFWAKE code were performed for conditions corresponding to the inboard propeller rotation data at the tow speed of 4.0 *knots*. The same data for axial and transverse velocities and turbulence kinetic energy which were used for the TWAKE simulations were used for initializing the present simulations with

SURFWAKE. As described in Appendix A, modifications were made to SURFWAKE to permit the code to accept empirical input data of this type.

The input data used by Swean [1] were for u, v, w and q on a uniformly spaced grid with $0.0 \leq y \leq 3.0$ ft and $-3.0 \leq z \leq 0.0$ ft and with 37 equally spaced grid points in each direction. The calculations were made for the starboard half plane of the flow field and a symmetry plane boundary condition was used on the left boundary representing the centerplane of the flowfield. In the TWAKE code, the variables are placed on the grid nodes, and the left column of grid points represents the plane of symmetry. In the SURFWAKE code, the staggered mesh scheme used for locating the dependent variables requires an extra column of points on the left boundary to implement a symmetry boundary condition. The actual plane of symmetry is the second column of grid points from the left with the left-most column of grid points being a column of image points.

The simulations with SURFWAKE used the same input data used by Swean [1] for u, v, w and q on a uniformly spaced grid with $-0.08333 \leq y \leq 3.0$ ft and $-3.0 \leq z \leq 0.0$ ft and with 38 equally spaced grid points horizontally and 37 points vertically. In the presentation of the results obtained with SURFWAKE, the dependent variables on the image grid column are shown for the the axial velocity, the turbulence kinetic energy, the transverse velocities and the principal Reynolds stresses. The reader will find that Swean [1] provides a very complete description of the initial plane data and for the variable distributions in the developing wake . The discussion which follows will thus be limited to describing the differences between the results of the present simulations and the differences between the present results and those of Ref. [1].

The initial distributions of axial excess velocity and turbulence kinetic energy, normalized by appropriate powers of the free stream velocity, are shown in Figs. 3a and 3b. The initial distributions of the transverse velocities, displayed in the alternate form of the nondimensional swirl velocity,

$$V_s \equiv \frac{1}{U_0}\left(v^2 + w^2\right)^{1/2},$$

are shown in Figs. 3c and 3d. The first of these is for the "rigid-lid" boundary condition and attention is called to the top row of points for which the velocity vectors are all horizontal. The second is for the linearized free surface boundary condition and it should be noted that on the top row, the velocity vectors are not all horizontal. With the linearized free surface boundary condition, the vertical velocity is determined from Eq. (17). As was noted above, a value was chosen for the dissipation scale length, ℓ_ϵ,

which gave a maximum value of the Reynolds stresses equal to the maximum value in the initial plane of the TWAKE simulation. The Reynolds stresses (initial conditions) are computed in the program from Eq. (5) using the experimental mean velocity and turbulence fields. The distribution of the resultant of the two principal Reynolds stresses,

$$\tau_r \equiv \frac{1}{U_0^2}\left((\overline{u'v'})^2 + (\overline{u'w'})^2\right)^{1/2},$$

is shown in Fig. 3e for the initial computational plane. With the exception of the additional column of points on the left boundary which is required to implement the symmetry plane boundary condition and the row of surface points in the linearized free surface option, the velocity input data shown in these figures are node for node identical to the input data for TWAKE in Ref. [1]. Since the Reynolds stresses are computed from the input data, and the models for the kinematic turbulent stresses are different in the two computer codes, the distribution for τ_r is slightly different from that given in Ref. [1].

In the figures that follow, the downstream development of the wake is shown for both types of free surface boundary conditions. Distributions for the velocity, turbulence kinetic energy and principal Reynolds stress are shown for $x = 16.0$ ft and 30.0 ft. The a) parts of the figures show the distributions for the "rigid-lid" boundary condition and the b) parts show the distributions for the linearized free surface boundary condition. For the sake of brevity, in the discussion of these figures, these boundary conditions will be refered to as the RL and LFS boundary conditions.

The distributions for the axial velocity are shown in Figs. 4 and 5 for 16.0 ft and 30.0 ft. In Fig. 4, very little difference is seen in either the drag wake of the hull or the overthrust wake wake of the propeller. At $x = 30.0$ ft, the drag wake decayed slightly less under the LFS boundary condition and the peak of the overthrust wake moved slightly downward and outboard.

The turbulence kinetic energy distributions are shown in Figs. 6 and 7. The differences at 16.0 ft are very slight. The peak value is slightly higher for the LFS boundary condition. At 30.0 ft the differences are more distinct. The peak value is about 5% higher for the LFS boundary condition and the location of the peak value is somewhat lower and more outboard than for the RL boundary condition.

The distributions of swirl velocity are shown in Figs. 8 and 9. At 16.0 ft, the swirl patterns in the propeller wake are quite similar with the maximum swirl velocity, V_{θ_m}, being about 9% higher for the LFS boundary condition. There is little difference in

the counter-rotating vortex above the propeller wake. For the RL boundary condition there is little development of a transverse velocity field away from the two principal vortices. For the LFS boundary condition, however, there is a distinct outward cross flow developing directed away from the main wake. At 30.0 ft, the values for V_{s_m} are the same to 1%. For the LFS boundary condition, the outward cross flow is nearly as strong as the swirl flow from the propeller, and the right boundary of the computational domain is not sufficiently far away. The development of the outward cross flow seems to be affected by the proximity of the right edge of the computational domain. As the cross flow approaches the right boundary, its direction changes from horizontal to vertically upward, and w is distinctly non-zero on the right boundary. For both boundary conditions, the counter-rotating vortex above the propeller wake has mostly disappeared.

The distributions of τ_x are shown in Figs. 10 and 11. At 16.0 ft, the distributions for the two boundary conditions are nearly identical, except for the top row. Along the top row, for the RL boundary condition, the stress vectors are directed inward toward a point above the propeller wake, and, for the LFS boundary condition, the stress vectors are directed outward and are in a direction opposite to the direction of the vectors on the row below. At 16.0 ft, the maxima of the resultant of the two principal Reynolds stresses, τ_{x_m}, are within 2.5% in the two simulations. At 30.0 ft, the peak value of τ_x is almost 10% greater with the LFS boundary condition. The surface row of points again displays opposite directions for the stress vectors, and for the RL boundary condition the stress resultant is greater with a larger vertical component on the two rows of points below the surface.

Distributions of axial velocity and turbulence kinetic energy in the surface plane of the simulations are shown in Figs. 12 and 13. These figures show the distributions for the full plane of the wake. The calculations were performed for the starboard half of the wake and data from the starboard half plane were reflected to the port half so that the wake for the full plane could be visualized. The velocity distributions show only small differences for the two boundary conditions. The wake decays slightly more rapidly with the RL boundary condition. The distributions of the kinetic energy of turbulence show that on the surface the the decay of the turbulence energy is more rapid with the LFS boundary condition. At 30.0 ft the level of turbulence kinetic energy in the surface plane is about 30% less with the LFS boundary condition than with the RL boundary condition.

The longitudinal development of the maximum and minimum values of the axial velocity and the turbulence kinetic energy are shown in Figs. 14 and 15 for the two surface boundary conditions. Fig. 14 shows distributions of the maximum axial velocity

in the wake, U_m, the minimum axial velocity in the wake, U_{min}, and the maximum axial velocity in the surface plane, U_{s_m}. The minimum velocity in the surface plane is identical to the minimum velocity in the wake. The maximum velocity in the wake is in the overthrust wake, the minimum velocity in the wake is in the drag wake of the hull and the maximum surface velocity is on the wake centerline where there is an overthrusted region in the initial plane data.

Fig. 15 shows the distributions of maximum turbulence kinetic energy in the wake, q_m, and on the surface, q_{s_m}. The peak in the turbulence is seen in the previous figures to be between the propeller overthrust wake and the hull drag wake where the gradients of the axial velocity are the greatest. The location of the maximum of the turbulence kinetic energy is consistently below the surface and in fact slowly moves downward with distance downstream.

A close comparison of the peak velocity distributions shows no difference in the maximum velocities. The minimum velocities do show some difference in that with the LFS boundary condition the hull drag wake decays less rapidly with downsream distance than with the RL boundary condition. For the turbulence kinetic energy distributions, it may be determined that the maximum turbulence in the wake decays less with the free surface boundary condition, whereas, as noted earlier, the maximum turbulence at the surface decays distinctly more rapidly with the LFS boundary condition.

The experimental data for the downstream stations have not yet become available. Comparison may readily be made with the results of the TWAKE simulations in Ref. [1]. Figs. 16a-16d are the results at $x = 30.0$ reported by Swean [1], and they show very close agreement with the computed results in the present simulation with the "rigid-lid" boundary condition (see Figs. 5a, 7a, 9a, 11a). The principal difference which is seen between the two sets of results is in the swirl velocity at $x = 30.0\ ft$. The present results showed that the upper outboard rotating vortex had essentially disappeared, whereas the results in Ref. [1] still showed a distinct vortex at that location. In the present simulation the maximum swirl velocity at 30.0 ft was 0.95% of U_0, while in the TWAKE simulation the decay of the swirl was slower and the maximum swirl was 1.35% of U_0. The more rapid decay of V_{s_m} may explain the more rapid disappearance of the upper clockwise vortex.

Principal measures of the wake development are given in Table 3a for $x = 16.0\ ft$ and in Table 3b for $x = 30.0\ ft$. These tables show the results for the TWAKE simulation in Ref. [1], and the present results for the "rigid-lid" and linearized free surface boundary conditions. The decline of the axial velocities was about the same in the three simulations. The peak of the propeller overthrust wake, U_m, decayed at the

same rate in the two present simulations and more rapidly than in the TWAKE simulation. The hull drag wake, U_{min}, decayed less rapidly in the SURFWAKE simulation and least rapidly with the linearized free surface boundary condition. The maximum of the turbulence kinetic energy, q_m, (which was located below the surface) decayed at the same rate in the three simulations. However, the maximum surface turbulence, q_{s_m}, decayed more rapidly with the SURFWAKE simulations and at about the same rate for the two boundary conditions. The maximum of the Reynolds stresses as indicated by τ_{x_m} decayed most rapidly in the TWAKE simulation and least rapidly in the SURFWAKE simulation with the linearized free surface.

Table 3. Comparison of Numerical Results

a). 16.0 ft

characteristic variable	TWAKE	SURFWAKE	
	RL b.c.	RL b.c.	LFS b.c.
U_m	7.44×10^{-2}	7.18×10^{-2}	7.18×10^{-2}
U_{min}	9.05×10^{-2}	1.01×10^{-1}	1.02×10^{-1}
q_m	4.15×10^{-3}	4.18×10^{-3}	4.25×10^{-3}
q_{s_m}	2.64×10^{-3}	1.81×10^{-3}	1.75×10^{-3}
V_{s_m}	2.74×10^{-2}	2.44×10^{-2}	2.66×10^{-2}
τ_{x_m}	1.23×10^{-3}	1.53×10^{-3}	1.57×10^{-3}

b). 30.0 ft

characteristic variable	TWAKE	SURFWAKE	
	RL b.c.	RL b.c.	LFS b.c.
U_m	4.13×10^{-2}	3.71×10^{-2}	3.65×10^{-2}
U_{min}	3.64×10^{-2}	4.29×10^{-2}	5.19×10^{-2}
q_m	1.92×10^{-3}	1.78×10^{-3}	1.76×10^{-3}
q_{s_m}	1.65×10^{-3}	1.19×10^{-3}	8.91×10^{-4}
V_{s_m}	1.35×10^{-2}	9.50×10^{-3}	9.59×10^{-3}
τ_{x_m}	4.38×10^{-4}	4.79×10^{-4}	5.27×10^{-4}

For the "rigid-lid" boundary condition the differences in the results are attributable to the differences in the turbulence models used in the two codes. Overall, the comparison of the three sets of results show very good agreement for the "rigid-lid" approximation of the free surface boundary condition. In the present simulations, the use of

the linearized free surface boundary condition has little effect on the axial velocities and a small effect on the turbulence kinetic energy. There is a distinct effect on the development of the transverse velocities. This effect on the evolution of the transverse velocities should be studied further.

Further Considerations

A basic purpose of this work was to evaluate the suitability of the SURFWAKE code for use in simulating wakes of surface ships. During the course of the work, several additional areas of concern developed and these concerns were addressed by additional calculations. In performing the simulations which have been presented above, the calculations were made only for the starboard half plane, since the wake centerline forms what should be a very natural plane of symmetry. Ref. [2] notes that any of the four sides of the computational domain may be set up as a plane of symmetry. In following the work of Swean [1] (and the physical location of the experimental data), the present simulations were naturally performed with a plane of symmetry on the left side. Calculations were perfomed for a full plane case to verify the appropriateness of approximating the full wake width by calculations for only the starboard half plane. The initial plane data were appropriately reflected across the centerplane, thus forming a set of data for the $x = 10.0\ ft$ initial plane which had 73 columns of data instead of the 38 columns for the half plane case and which was truly symmetrical with respect to the centerplane.

The transverse velocity distributions for $x = 30.0\ ft$ are shown in Fig. 17. The distribution for the full plane is shown in Fig. 17a. Along the center column and directly above the center of the propeller vortices can be seen some evidence of local asymmetry. By expanding the scale of the plots, i.e. by plotting each half of the full plane flowfield separately, differences in the two sides can be seen more clearly. Fig. 17b shows the port half of the flowfield and Fig. 17c shows the starboard half. In these latter two figures, it is more easily seen that some of the velocity vectors in the centerplane have a lateral component. It may also be seen that the columns to each side of the centerplane do not quite match each other. Elsewhere in the flow field, asymmetries are not readily seen. By considering the two halves of the flowfield separately, it was also determined that the peak swirl velocity V_{s_m} was 0.995% U_0 for the port half plane and 0.964% U_0 for the starboard half plane.

The reason for asymmetries developing in the flow simulation is clearly in the numerical method. All of the dependent variables are center-differenced. However, most of the flow variables are assigned locations at the center of the cells of the computational grid while the v and w components of the velocity are assigned locations on the

faces of the grid cells. The apparent result is that small differences may be expected to be found between the port and starboard halves of a full plane calculation when the SURFWAKE code is initialized as it was for these simulations. However, the overall accuracy of the simulation for either half of the flow field seems to be quite satisfactory. Comparison of Fig. 17c with Fig. 9a shows only very small differences.

Another area of concern arose during the course of the free surface calculations. In Fig. 9b, for the linearized free surface boundary condition, it was noted that the transverse velocities were not sufficiently small at the right boundary of the computational domain. Clearly, simulations with the free surface boundary condition which extended further downstream would be contaminated by the transverse velocity components not vanishing on the right side. The boundary conditions for the right side and for the bottom require that the dependent variables vanish on those boundaries. Two remedies were readily available. The code contained a provision for a wave damper which could be easily activated. A slight change in the coding was made to permit the wave damper to be applied only at the side that was not being used as a symmetry plane. The distribution of transverse velocities at $x = 30.0\ ft$ from a simulation using the wave damper is shown in Fig. 18a. The wave damper is set to affect the five rightmost columns of grid points. The damping is clearly effective in preventing the non-zero tranverse velocities from reaching the right boundary. In fact, the damping causes an excessively large change in the transverse velocities between the fifth and sixth columns of grid points. The amount of the damping can be adjusted, but this option was not explored.

A second remedy for the velocity field interacting with the right boundary is expansion of the computational domain. The domain is most easily expanded by adding additional columns of points to the right side. A simulation was made with double the number of grid points in the lateral direction. The tranverse velocity distribution for $x = 30.0\ ft$ from that simulation is shown in Fig. 18b. While the flowfield has not reached the outer boundary, contamination of the right boundary would be expected to occur, if the simulation were extended to 60.0 ft. The expanded grid required nearly a doubling of computer time for the simulation.

The free surface boundary conditions shown in Eqs. (14) - (18) are correct for linear gravity waves. However, due to the parabolic nature of the solution technique, it is not clear that the code is capable of generating surface elevations that resemble the classic Kelvin wave pattern. Certainly the transverse wave system will never appear. Using the results from the current simulation, the free surface elevation may be calculated two ways. First, Eq. (16) states that the wave amplitude is directly proportional to the axial excess velocity component. Plots of the surface values of the axial velocity are shown

in Fig. 12b for values of x from 10.0 to 30.0 $ft.$ and in Fig. 19a for values of x from 10.0 to 190.0 $ft.$ These figures are characteristic of a single wave crest on each side of the plane of symmetry, not diverging Kelvin waves. The second method for determining the wave elevation is consistent with the method of Ref. [2] for determining the value of variables at the $n+1$ time step given their values and their derivatives at the n^{th} time step. For the wave elevation, this would be

$$\eta^{n+1} = \eta^n + \Delta x \frac{\partial \eta^n}{\partial x} + \frac{(\Delta x)^2}{2} \frac{\partial^2 \eta^n}{\partial x^2} \tag{19a}$$

or, using Eq. (14),

$$\eta^{n+1} = \eta^n + \Delta x \frac{w^n}{U} + \frac{(\Delta x)^2}{2U} \frac{\partial w^n}{\partial x} \tag{19b}$$

The results of this calculation are shown in Fig. 19b for values of x from 10.0 to 190.0 $ft.$ The wave damper was active which yielded zero wave heights at the outer boundary. Again the detail of the transverse wave system is lacking. The manner in which SURFWAKE can be used to give realistic wave profiles should be the topic of a future study.

Expansion of the computational domain by using a variably space grid is an option that could be considered. Some experience with a variably space grid has shown that extra care is needed in obtaining correct dependent variable values on the surface and symmetry plane boundaries. There was also the intent to maintain a high level of similarity between the present work and that of Swean [1]. Thus, the option of employing a variably spaced grid was not explored in the present work.

4. SUMMARY

The results which were obtained in the present simulations using the SURFWAKE code with the "rigid-lid" approximation for the free surface boundary condition agreed well with the results which Swean [1] obtained with the TWAKE code. The results for the linearized free surface boundary condition agreed well for the axial velocities and for the turbulence kinetic energy. The differences in the transverse velocities were large but seemed to have only small effects on the evolution of the axial velocity distributions or the distributions of turbulence kinetic energy. In the SURFWAKE code, the axial momentum conservation equation is linearized and as a result the code is not appropriate for use when the wake drag or overthrust velocities are not small with respect to the free stream velocity. SURFWAKE does have a significant advantage compared

to TWAKE with respect to CPU requirements. The computations in the present work required on the order of a tenth of the computer times that are required with TWAKE. This is because of the explicit algorithm and the linearization used in the SURFWAKE code. While the code requires a smaller marching step-size for stability there is no requirement for the formation of the large Jacobian and subsequent matrix inversion. Overall, the SURFWAKE code seems quite suitable for wake calculations when the "rigid-lid" approximation for the free surface boundary condition is used. However, the linearized free surface boundary condition seems to give poor simulations for the transverse velocities. Further work is needed with the linearized free surface boundary condition.

5. ACKNOWLEDGEMENTS

The authors acknowledge the support of the Office of Naval Research (Code 12), the Naval Research Laboratory, the David Taylor Research Center, and the University of Michigan for the support for this project through the Ship Wake Consortium.

6. REFERENCES

[1] T. F. Swean, Jr.,"Numerical Simulations of the Wake Downstream of a Twin-Screw Destroyer Model," NRL Memorandum Report 6131, December 1987.

[2] J. C. S. Meng and G. E. Innis, "User's Manual for the Computer Code FAST-WAKE: A Fast and Accurate Code for Simulation of the Stratified Turbulent Wake Flows Part I: Fundamental Structure," Report SAI - 77 - 864 - LJ, Science Applications, Inc., 1977.

[3] J. W. Rottman, L. Y. Oey, J. C. S. Meng and J. R. Grant, "A Computational Model for Turbulent Wake Flows in A Stratified Fluid Part I: Fundamental Formulation," Report SAI - 200 - 79 - 986 - LJ, Science Applications, Inc., 1980.

[4] J. R. Grant, G. E. Innis and W. Y. Shaw, "A Computational Model for Turbulent Wake Flows in A Stratified Fluid Part II: Numerical Simulation of Wakes behind towed and Self-Propelled Axisymmetric Bodies," Report SAI - 200 - 80 - 483 - LJ, Science Applications, Inc., 1980.

[5] J. C. S. Meng, J. R. Grant, and J. S. Uhlman, Jr., "Numerical Simulation of Turbulent Wake With a Free Surface," Gould Defense Systems, Inc., GOULD OSD-771-HYDRO-CR-85-05, Oct., 1985.

[6] W. T. Lindenmuth, private communication to T. F. Swean, Jr.: data from the model experiments at DTRC - outboard propeller rotation, Aug. 1986.

[7] W. T. Lindenmuth, private communication to T. F. Swean, Jr.: data from the model experiments at DTRC - inboard propeller rotation, Jan. 1987.

[8] R. K. C. Chan, "Two-Dimensional Time-Dependent Calculations of Large-Amplitude Surface Gravity Waves Due to a Surface Disturbance," Proc. First International Conf. Ship Hydro., 1975.

APPENDIX A – Input data for SURFWAKE

For the purposes of this Appendix, the modified code will be distinquished from the original program SURFWAKE by the name SURFWAKE.v2. Many of the input variable names for the program SURFWAKE.v2 follow the definitions given by Meng and Innis [2] and Meng et al. [5]. Additions and changes to the orginal I/O variables are noted here. Generally, lower case characters are used to identify the differences between SURFWAKE and SURFWAKE.v2. For a more complete description of the parts of the program that are unchanged, the user is referred to the above references.

The program SURFWAKE.v2 has options that allow the user to input part or all of the program parameters. The initial plane data for the wake can also be calculated or read in. This is useful if experimental data exist for the hull-form being studied. Input is read from the various input files (tapes) in either NAMELIST, formatted READ statements, or unformatted READ statements. Output is written to files (tapes) as described below. The different I/O device numbers, the NAMELIST variables and the formatted/unformatted input variables are described in the following sections. The output variables essentially follow the description given by Meng and Innis [2].

I/O Device Numbers

Device number 5 and device number 6 are reserved for the default input and output devices respectively. The other I/O devices in SURFWAKE.v2 are set in the OPEN commands listed below. Each command and device number is given with a brief description.

`open (unit= 8,file='to be user specified',form='formatted',status='old')`
Device 8 is for fixed grid, initial wake plane input read in SUBROUTINE DATAIN and SUBROUTINE SETUP1. The data are not interpolated onto a new computational grid. The downstream grid remains unchanged from the one read in.

`open (unit=10,file='tape10',form='unformatted',status='unknown')`
Device 10 contains summary information of output. The variables are written from SUBROUTINE PRINT and read in SUBROUTINE RTAPE.

`open (unit=11,file='tape11',form='unformatted',status='unknown')`
Device 11 contains current values from the full blank COMMON block. The variables are written from SUBROUTINE WTAPE and SUBROUTINE PRINT and read in SUBROUTINE RTAPE.

`open (unit=12,file='tape12',form='unformatted',status='unknown')`
Device 12 contains output of the free surface elevation, ETAA. The values are written in SUBROUTINE BOUND7.

`open (unit=14,file='tape14',form='formatted',status='unknown')`
Device 14 contains output for surface contours written to a file from SUBROUTINE PRINTSUR.

`open (unit=15,file='tape15',form='formatted',status='unknown')`
Device 15 contains output of the maximum values of the variables from SUBROUTINE PRINTMAX and SUBROUTINE DATAIN.

`open (unit=16,file='tape16',form='formatted',status='unknown')`
Device 16 contains output of the maximum values of the variables on the free surface from SUBROUTINE PRINTSMAX.

Input via NAMELIST Statements

NAMELIST variables are read in on device 5. They are separated into four groups with group-names of "namer1", "group2", "group3", and "group4". The variable names, types, definitions, and default values are shown in Table I. In this table, the vessel beam is denoted by the symbol B.

Table I.1 NAMELIST /namer1/ Variables

Variable	*Type*	*Definition*	*Default Value*
restrt	Integer	Run control flag; set equal to 0 for new run. Set equal to 1 to restart the program reading the last COMMON blocks from tape.	None
IRCYCL	Real	Restart information, the cycle number from which the problem is to be continued.	None

Table I.2 NAMELIST /group2/ Variables

Variable	*Type*	*Definition*	*Default Value*
B1	Real	Grid parameter: stretch coefficient in y-direction.	0.16334881
B2	Real	Grid parameter: stretch coefficient in z-direction.	0.14207855
CONDUC	Real	Thermal diffusivity, normalized by beam, B.	0.0
CZERO	Real	Maximum value of concentration at wake center.	1.0
DIST	Real	Integral length scale for turbulence, l_d, normalized by B.	0.22
DT	Real	Initial marching increment, normalized by B.	0.1
DVDZSH	Real	Transverse shear gradient, normalized by U_0/B.	0.0
DYMIN	Real	Minimum mesh size in the y-direction, normalized by B.	0.05
DZMIN	Real	Minimum mesh size in the z-direction, normalized by B.	0.05
FNUM	Real	Internal "Froude number" based upon body speed, beam, and Brunt-Vaisala frequency.	32.0
FREE	Integer	Free surface control flag; set equal to 1 for a free surface on $z = 0$ otherwise set equal to 0.	0

Variable	*Type*	*Definition*	*Default Value*
FULL	Integer	Run control flag: 0 = Use default values set in SUBROUTINE DEFINE for input ; 1 = Calculate subsurface initial plane wake profiles as described by Ref. [5]; 2 = Calculate surface initial plane wake profiles as described by Ref. [5]; 3 = Data input on unit 5 for u, v, w, and q. These values will be used for the interpolated grid defined in SUBROUTINE SETUP1. SUBROUTINE SETUP6 will be called instead of SUBROUTINE SETUP5. 4 = Data input on unit 8 for u, v, w, and q. The values are read in SUBROUTINE DATAIN. They will be used on the (y, z) grid points read in from device 8 in SUBROUTINE SETUP1. SUBROUTINE SETUP6 will be called instead of SUBROUTINE SETUP5. With this option, the grid will not be rescaled. The input grid will be used in all the downstream computations.	0
G	Real	Gravitational acceleration, normalized by $U_0 * U_0/B$. Equivalent to the reciprocal of the square of the Froude Number based upon the beam.	12.3
ICEN	Integer	Cell index I closest to wake center.	24

Variable	*Type*	*Definition*	*Default Value*
IDUM(20)	Integer	Control flag: IDUM(1)...IDUM(19) determines which variables will be output in line printer contour plots on device 6. For M plots (M .LT. 19), IDUM(1)...IDUM(M), should be assigned values in accordance with the BLOCK PRINT identifiers shown below. IDUM(M+1) must be set equal to 0. IDUM(20) controls the number of calls to the SUBROUTINE INICON. When IDUM(20) equals 1 the second call to SUBROUTINE INICON will be skipped. See Ref. [2] for the justification behind calling INICON twice.	IDUM(1) = 0

BLOCK PRINT identifiers for IDUM variables
notation as used in SUBROUTINE PRINT thus u'v' elsewhere appears here as U*V*

1 Q	2 U*	3 V*	4 W*	7 U*V*
8 U*W*	9 R*W*	10 R*W*	11 RHO*	12 C
13 U	14 V	15 W	16 PHI	17 RS
18 RHO	19 E	20 QS	21 ES	22 V*W*
23 Q*V*	24 Q*W*	25 E*V*	26 E*W*	27 C*V*
28 C*W*				

IMAX	Integer	Maximum number of zones in the y-direction including fictitious zones.	47

Variable	*Type*	*Definition*	*Default Value*
ITEST	Integer	Flag to determine form of selective editing in the data print out on device 6 after NFREQE steps: 0 = turbulence and mean flow data 1 = mean flow data 2 = data in scratch arrays A1-A5, PHI, RHOEQL, VSHEAR	0
IZONE	Integer	Number of zones included in the wave damper along the vertical edges of the computational domain.	5
JCEN	Integer	Cell index J closest to wake center.	23
JMAX	Integer	Maximum number of zones in the z-direction including fictitious zones.	45
MAXCYC	Integer	Maximum number of cycles allowed for computation.	2000
NFLAG	Integer	Control flag set equal to 0 to read in probe positions otherwise set equal to 1.	0
NFREQB	Integer	Number of longitudinal time steps between line printer plots. (Equivalent to number of calls to SUBROUTINE BLOCKP.)	2000
NFREQD	Integer	Number of longitudinal time steps between probe displacement calculations.	1

Variable	*Type*	*Definition*	*Default Value*
NFREQE	Integer	Number of longitudinal time steps between calls for output by **SUBROUTINE EDIT**. Recommend use of a large value of **NFREQE** to prevent **EDIT** outputs.	1000
NFREQF	Integer	Number of longitudinal time steps between writes of flow field information on the transverse plane to tape11.	15
NFREQL	Integer	Number of longitudinal time steps between calculation of power law	10
NFREQP	Integer	Number of longitudinal time steps between flow field short summary output.	1
QZERO	Real	Maximum value of turbulence energy at wake center, normalized by $U_0 * U_0$.	0.00366
T	Real	Downstream distance at initial plane, normalized by B.	10.0
TEXPND	Real	Downstream distance at which rezone will be performed, normalized by B.	2000.0
TIMEMX	Real	Distance downstream at which run will be terminated if **MAXCYC** has not been reached, normalized by B.	300.0
UD	Real	Maximum axial velocity excess normalized by U_0	0.082
VISCOS	Real	Molecular viscosity coefficient, normalized by BU_0 so that VISCOS $= 1/ReB$.	0.0000333
VISMAX	Real	Maximum damping coefficient in wave damper along vertical boundaries.	0.0

Variable	*Type*	*Definition*	*Default Value*
VSWIRL	Real	Maximum swirl, normalized by U_0.	0.0338
YMAX	Real	Maximum y-dimension of the computational grid. Used in Type-2 or Type-3 zoning in SUBROUTINE SETUP1.	None
YZERO	Real	Y-distance from center of cell (ICEN,JCEN) to axis system fixed at wake center, normalized by Δy_{min}.	None
ZMAX	Real	Maximum z-dimension of the computational grid. Used in Type-2 or Type-3 zoning in SUBROUTINE SETUP1.	None
ZZERO	Real	Z-distance from center of cell (ICEN,JCEN) to axis system fixed at wake center, normalized by Δz_{min}.	0.0
Z12	Real	Bottom boundary of first region of constant density stratification.	100.0
Z23	Real	Bottom boundary of second region of constant density stratification.	-100.0

The last two NAMELISTs, NAMELIST/group3/ and NAMELIST/group4/, are associated with the generation of initial plane data for subsurface and surface vessels respectively. The various wake generating components are identified and their contributions linearly superimposed on the first downstream computational grid. The rationalization for this procedure and a brief description of the variables in the NAMELISTs are given by Meng, et al. [5]. They will not be repeated here.

Input via READ Statements

The following four READ statements are executed in SUBROUTINE CARDSNL:

```
read (5,namer1)
read (5,group2)
read (5,group3)
read (5,group4)
```

They reference the NAMELIST statements described in the previous section. The proper syntax rules for NAMELIST input should be followed.

When the NAMELIST/group2/ variable FULL equals 1, 2, or 3, experimental data may be read in and seeded onto the program generated grid. The experimental quantities may be one or more of the following one-dimensional variables:

RHOAMB,	the initial ambient stratified density profile normalized to be unity at the wake center, or
VSHEAR,	the shear velocity distribution normalized by the uniform stream velocity U_0

or one or more of the two-dimensional variables:

C,	the dye concentration,
Q,	the turbulence kinetic energy normalized by $U_0 * U_0$,
RHO,	the total local fluid density normalized by the dimensional value of the ambient density at the wake center,
U,	the streamwise perturbation velocity normalized by U_0,
V,	the horizontal velocity normalized by U_0, or
W,	the vertical velocity normalized by U_0.

The first line for the experimental data is read in SUBROUTINE DATAIN by the following READ statement:

```
      READ (5,1000) TITLE,IFLAG,NDAT,iprn
1000 FORMAT(A8,3I5)
```

where

TITLE is a descriptive title for the data or "END" for the last line of the experimental input. This card must be included even if FULL = 0.

IFLAG is the input variable identifier :

1 = RHOAMB
2 = VSHEAR
3 = C
4 = Q
5 = RHO
6 = U
7 = V
8 = W

NDAT is the number of input data values.

iprn is a variable to control the printing of the input values for the IFLAG variable on device 6.
Set iprn = 1 for printing, = 0 for no printing.

If IFLAG equals 1 or 2 (one-dimensional input) then the following READ statement is executed:

```
      READ (5,1005) (ZIN(I),DATIN(I),I=1,NDAT)
1005 FORMAT(8F10.0)
```

Otherwise, for IFLAG equal to 3 - 8 (two-dimensional input) the READ statement is

```
      READ (5,1007) (YIN(I),ZIN(I),DATIN(I),I=1,NDAT)
1007 FORMAT(6F10.0)
```

where (YIN,ZIN) are the (y, z) coordinates of the IFLAG variable and DATIN is the actual value of the variable. The data points must be read in sequence of ZIN monotonicly increasing for one dimensional arrays. For two dimensional arrays, the order is arbitrary.

When the NAMELIST/group2/ variable FULL equals 4, experimental data for a fixed grid and the fixed grid coordinates are to be read in from device 8. The experimental data is entered in SUBROUTINE DATAIN and the grid coordinates are entered in SUBROUTINE SETUP1. The first lines in the file attached to device 8 contain the grid points. They are read in SUBROUTINE SETUP1 by the following statements:

```
read (8,*) imax
do i = 1, imax
    read(8,*) y(i)
end do
```

and

```
read (8,*) jmax
do j = 1, jmax
    read(8,*) z(i)
end do
```

The experimental quantities must be the two-dimensional variables: u, q, w, and v. To read them into the program, the following statements are executed in SUBROUTINE DATAIN:

```
      do i = 1, imax
         do j = 1, jmax
            k = k + 1
            read (8,690) u(k),q(k),w(k),v(k)
690   format(4e15.7)
         end do
      end do
```

The point (i,j) = (1,1) corresponds to the lower left corner of the grid and the point (i,j) = (imax,jmax) corresponds to the upper right corner. The data are read in row by row.

After the initial plane variables described above have been read in from device 5 or device 8, the following READ statement is executed in SUBROUTINE PRINT:

```
      READ (5,15) (TITLE(I),I=1,20)
   15 FORMAT(20A4)
```

where TITLE is the identifying title of the run.

If NFLAG = 0 , then an initial call is made to SUBROUTINE DIPSCAL to read in experimental probe locations. SUBROUTINE DIPSCAL will compute the isopycnic displacement at those locations [2]. The locations are read in on device 5 with the following READ statement:

```
      READ (5,1) NPROBE
    1 FORMAT (I10)
      DO 5 N = 1, NPROBE
         READ (5,2) YPROBE(N), ZPROBE(N)
    2 FORMAT (2E10.2)
    5 CONTINUE
```

See Appendix F of Ref. [2] for details when using this option.

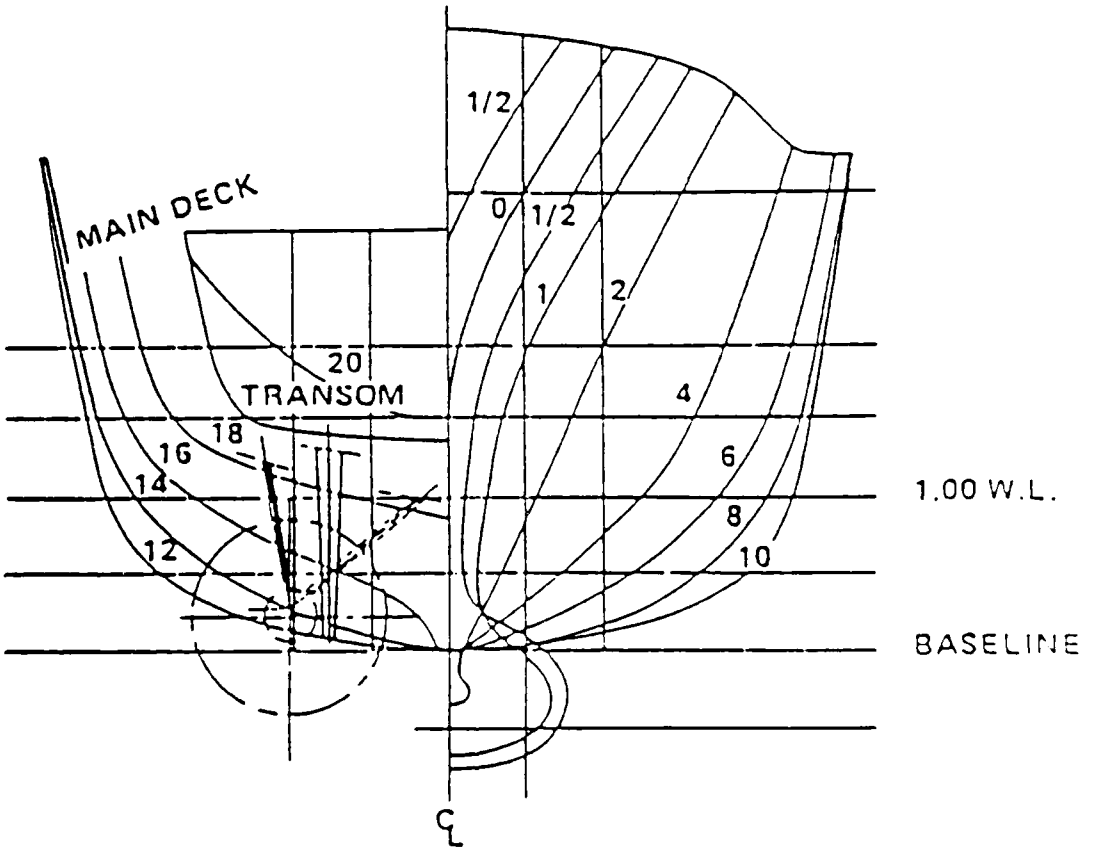

Fig. 1 – Body plan for high speed ship

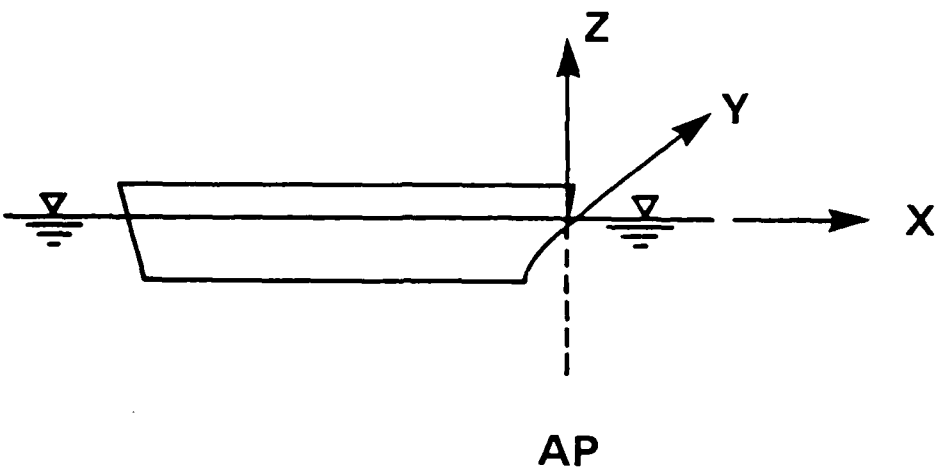

(a) model coordinate system

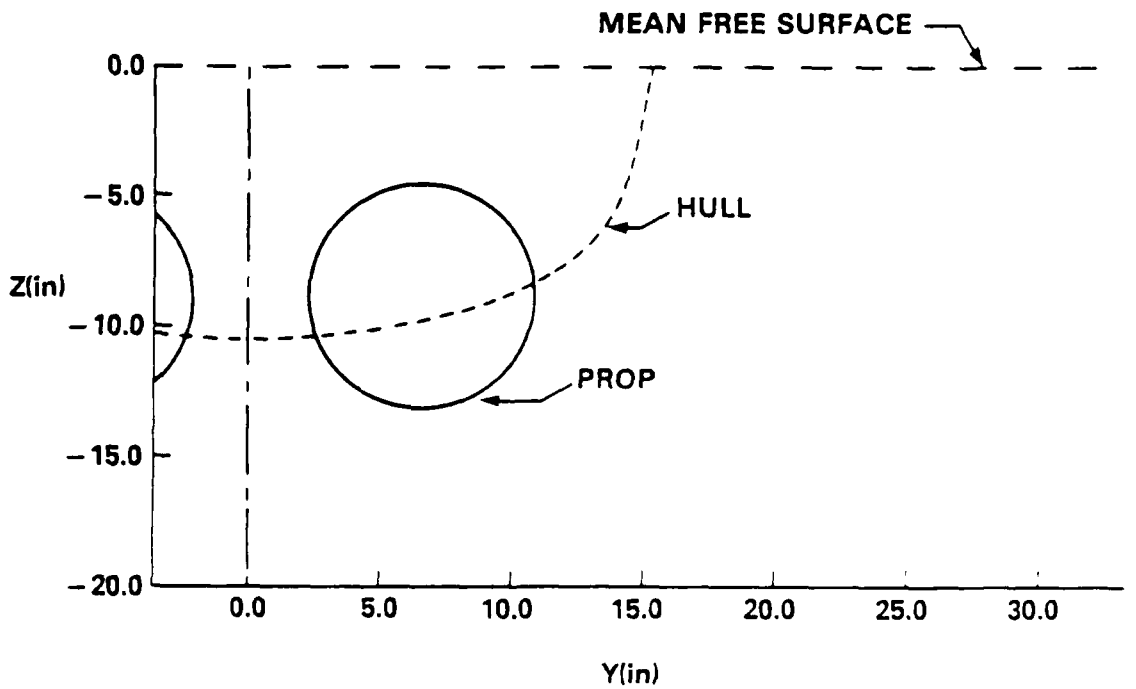

(b) typical measurement domain

Fig 2 – Schematics of model coordinate system and transverse plane measurement domain

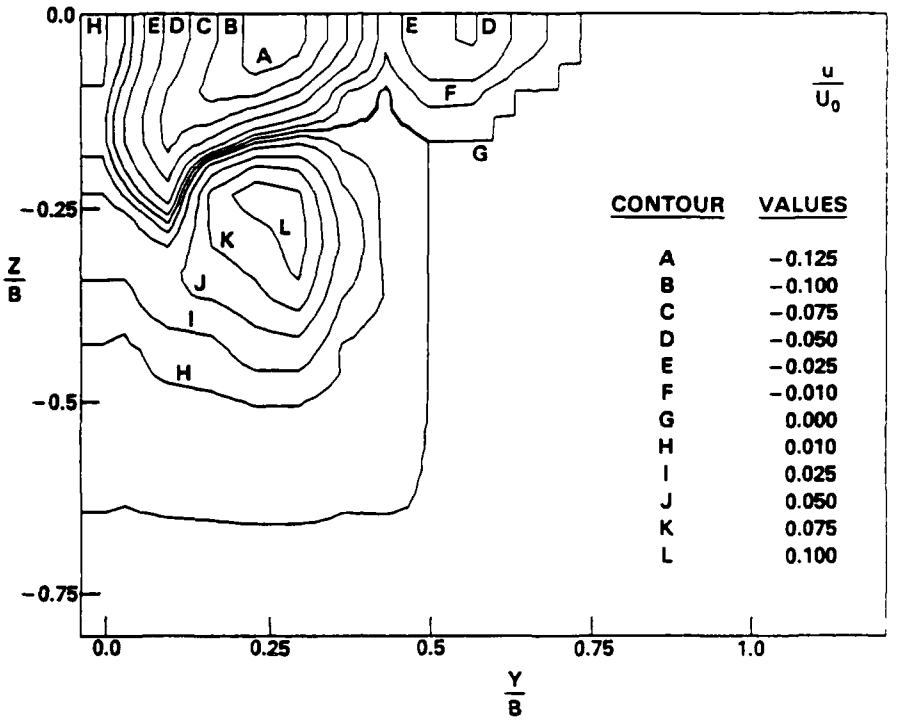

(a) contours of mean streamwise velocity

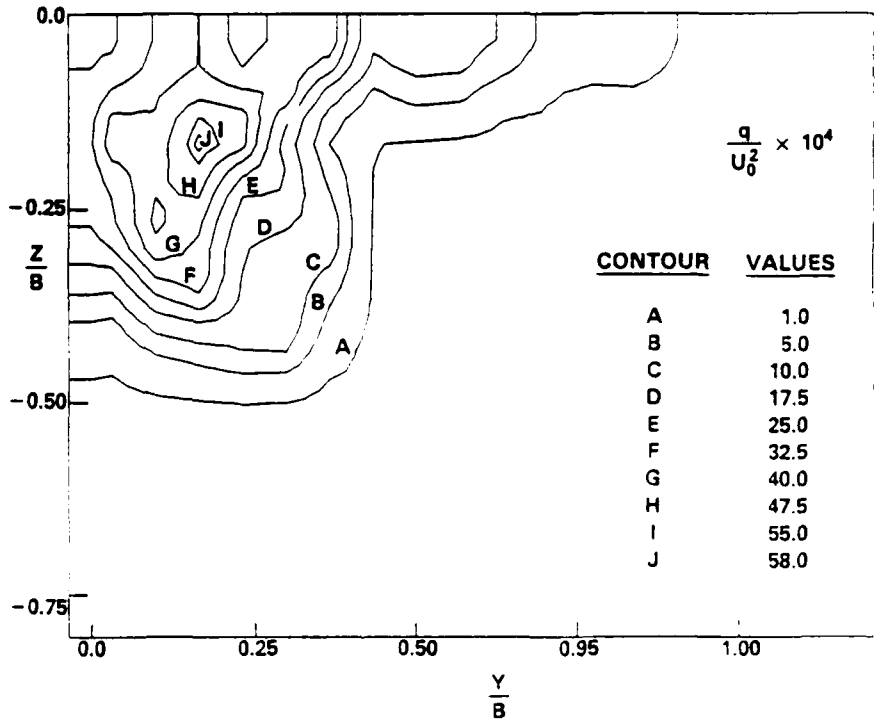

(b) contours of turbulence kinetic energy

Fig. 3 – Distributions of Initial Profile Data – $x = 10.0$ *ft*

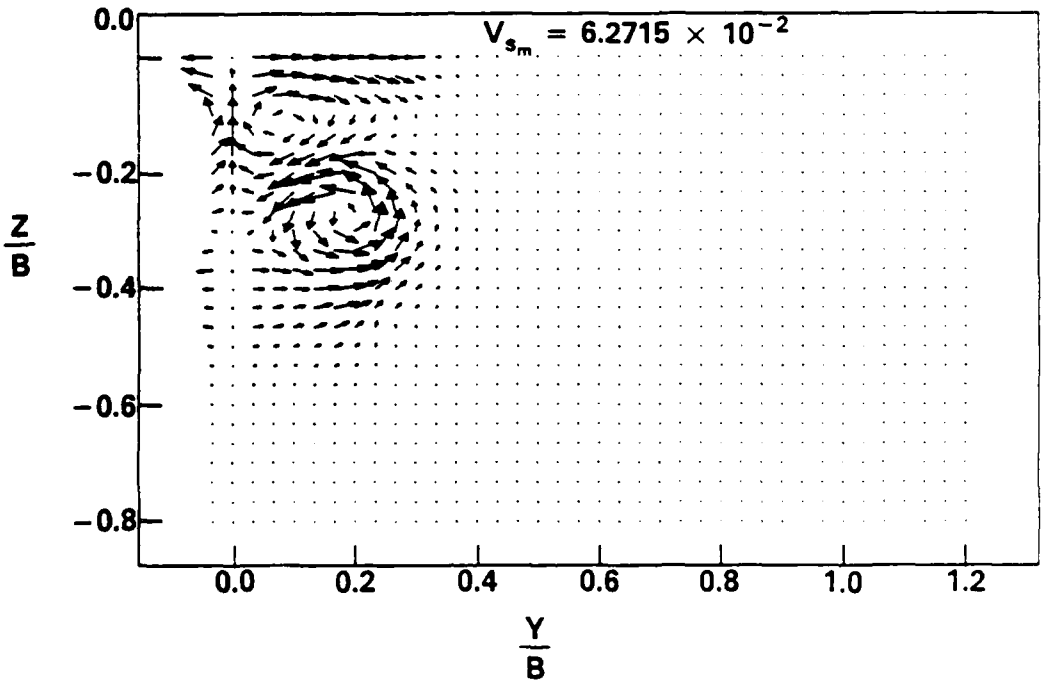

(c) swirl velocity vectors – "rigid-lid" surface boundary condition

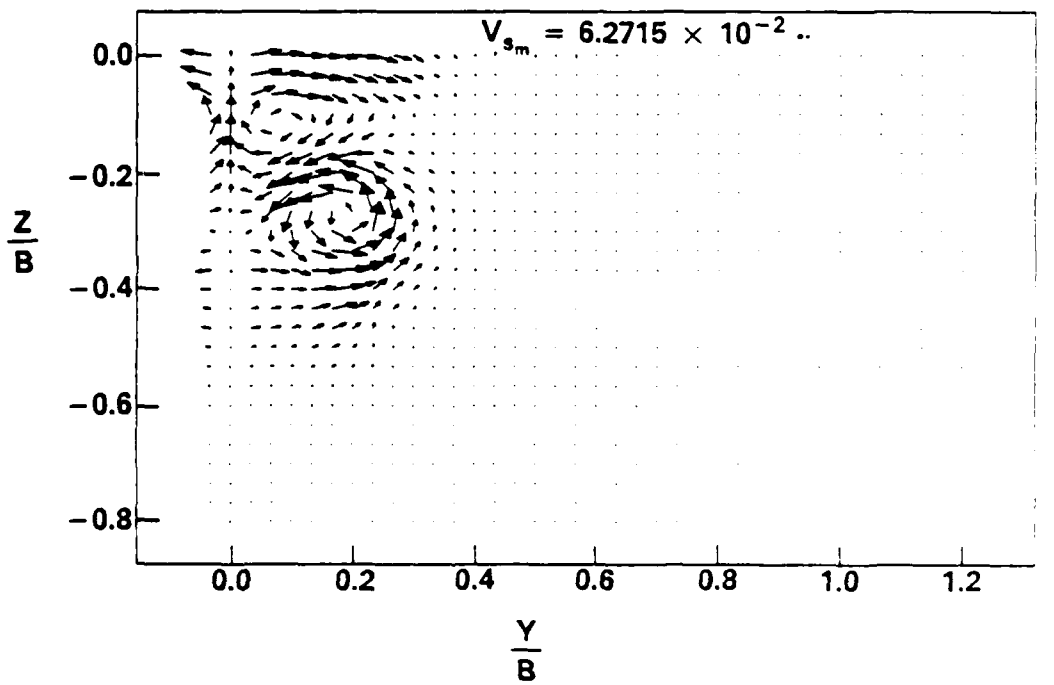

(d) swirl velocity vectors – linearized free surface boundary condition

Fig. 3 (Cont'd) – Distribution of Initial Profile Data – x = 10.0 ft

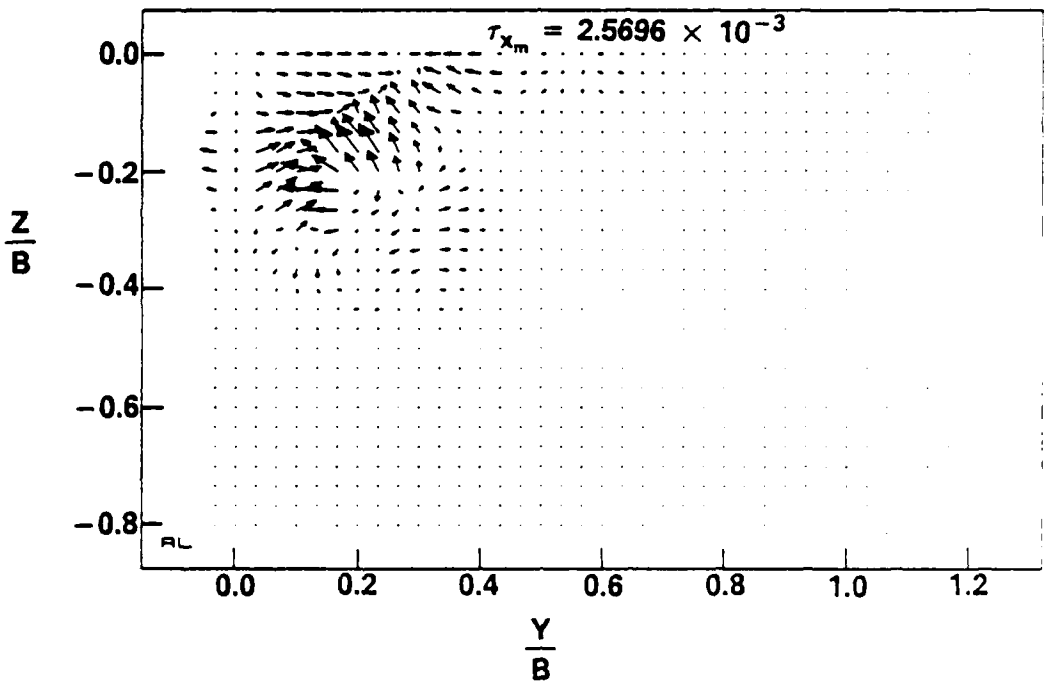

(e) Reynolds stress distribution

Fig. 3 (Cont'd) – Distribution of Initial Profile Data – $x = 10.0$ *ft*

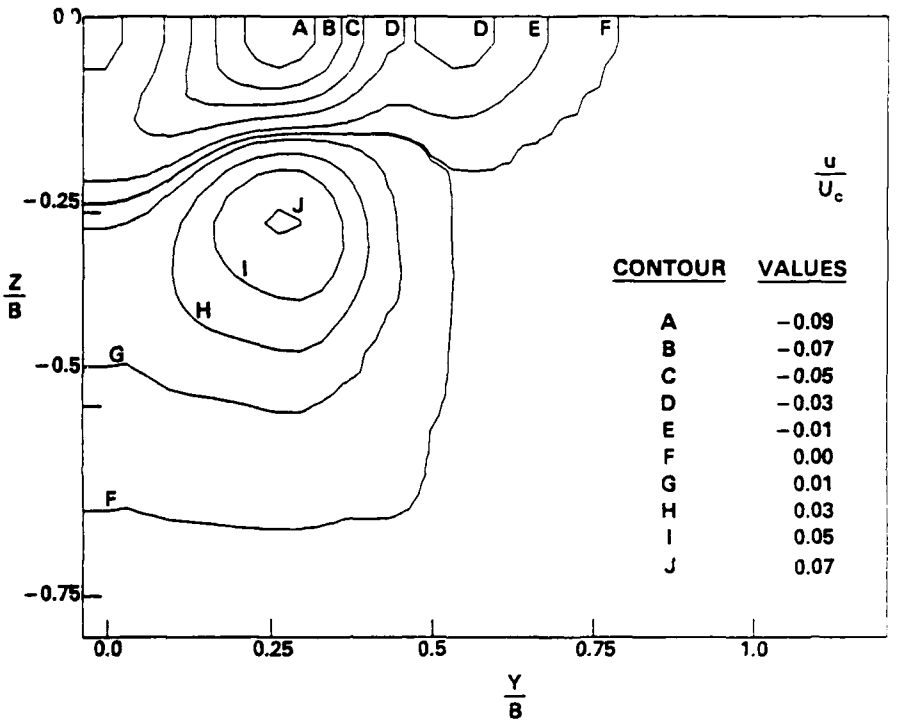

(a) "rigid-lid" surface boundary condition

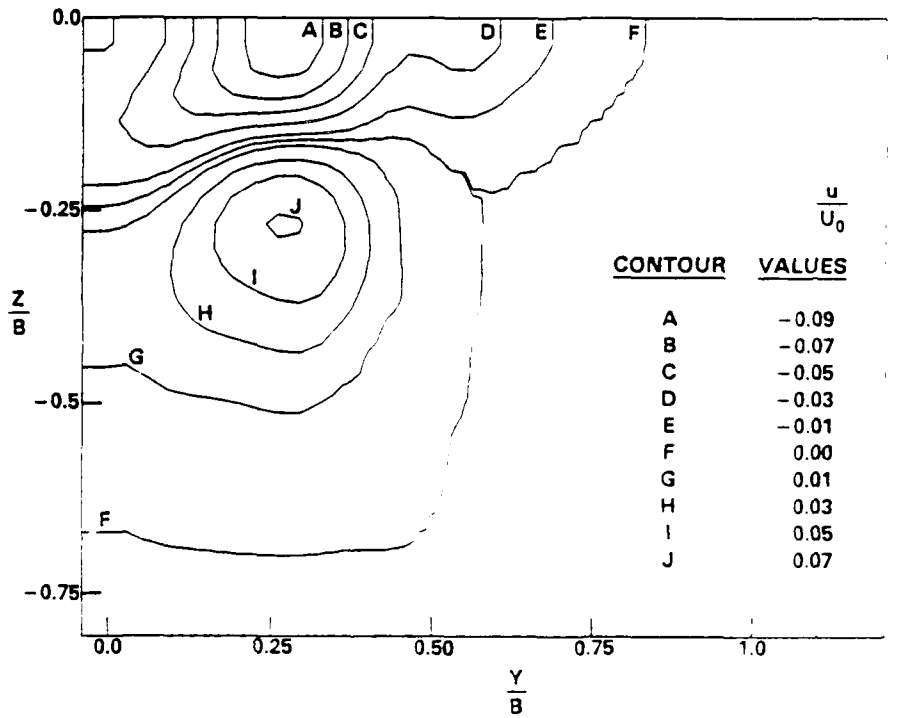

(b) linearized free surface boundary condition

Fig. 4 – Contours of mean streamwise velocity $x = 16.0$ ft

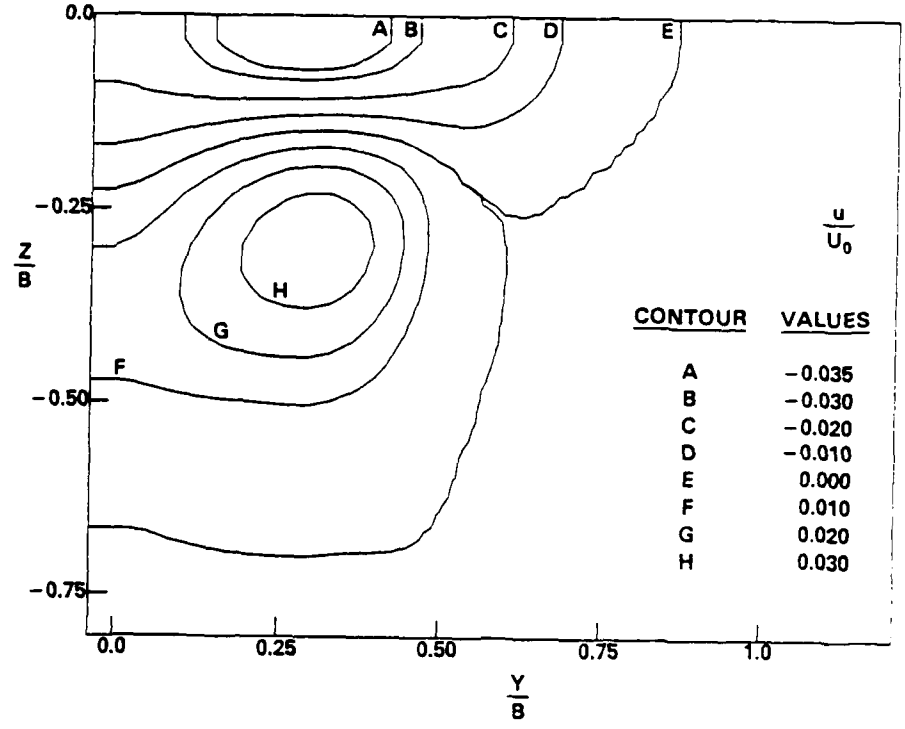

(a) "rigid-lid" surface boundary condition

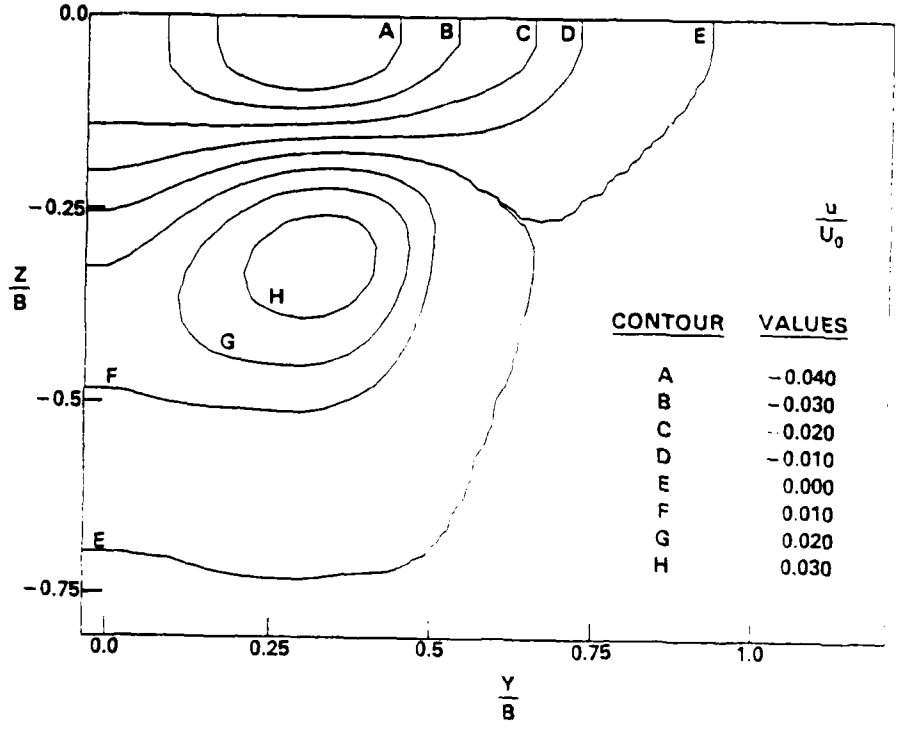

(b) linearized free surface boundary condition

Fig. 5 – Contours of mean streamwise velocity $x = 30.0$ *ft*

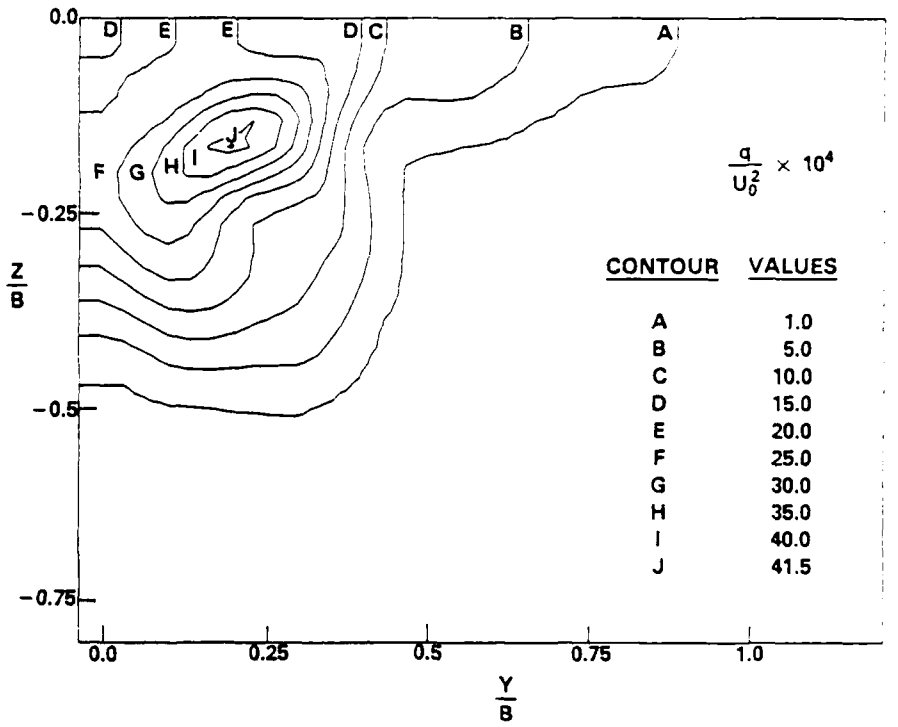

(a) "rigid-lid" surface boundary condition

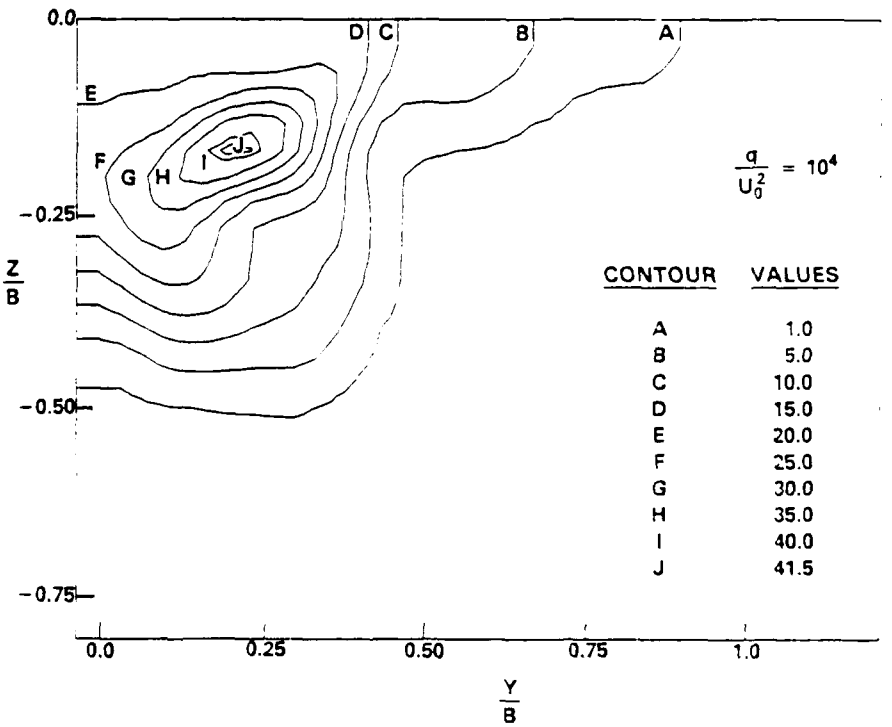

(b) linearized free surface boundary condition

Fig. 6 – Contours of turbulence kinetic energy $x = 16.0$ ft

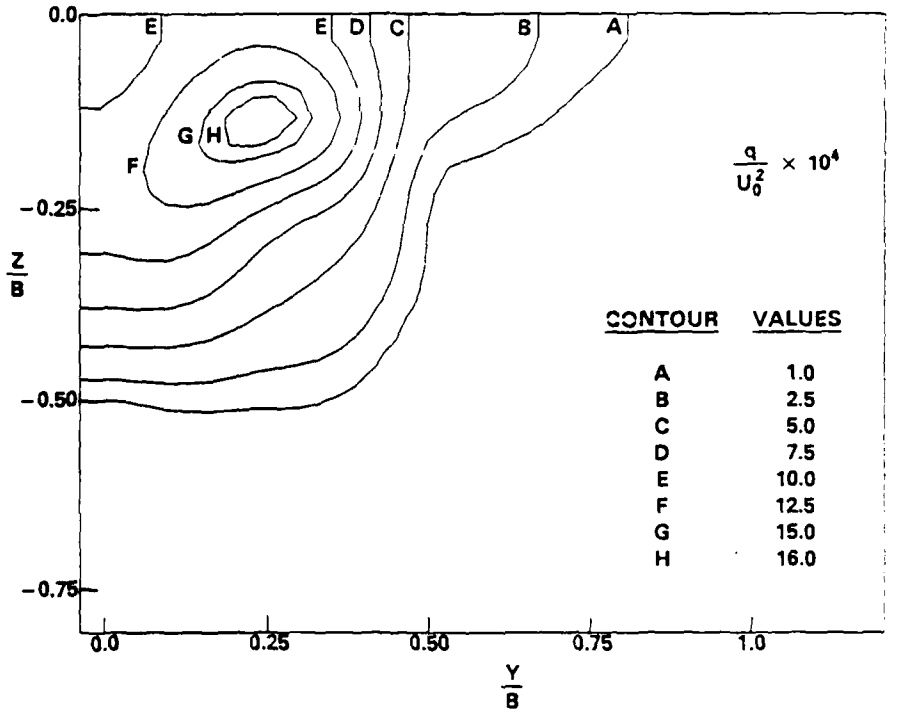

(a) "rigid-lid" surface boundary condition

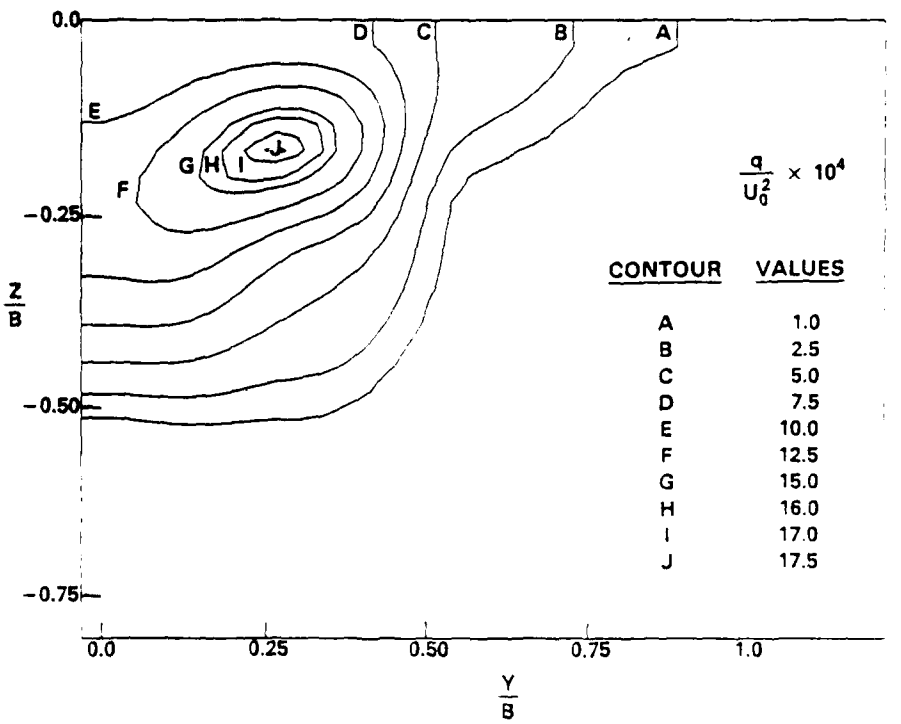

(b) linearized free surface boundary condition

Fig. 7 – Contours of turbulence kinetic energy $x = 30.0$ *ft*

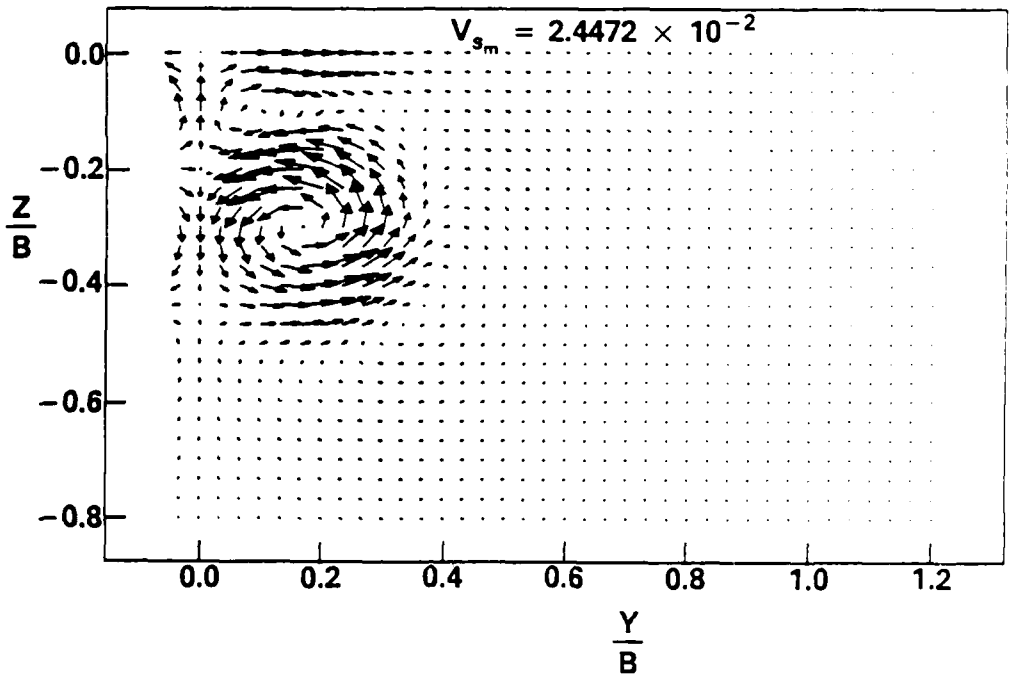

(a) "rigid-lid" surface boundary condition

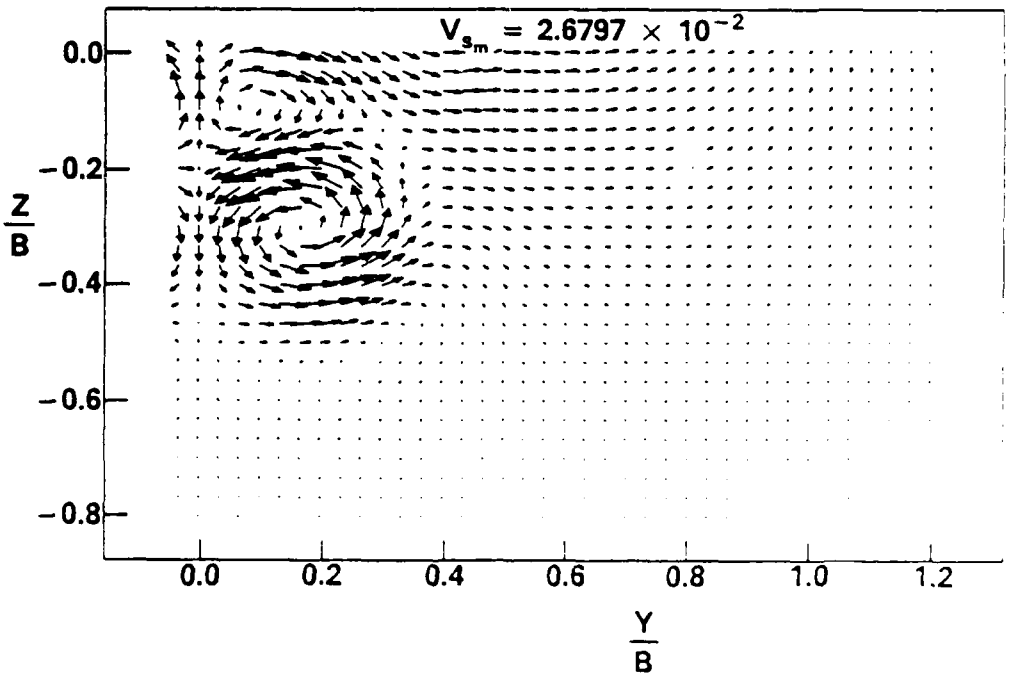

(b) linearized free surface boundary condition

Fig. 8 – Swirl velocity vectors τ = 16.0 *ft*

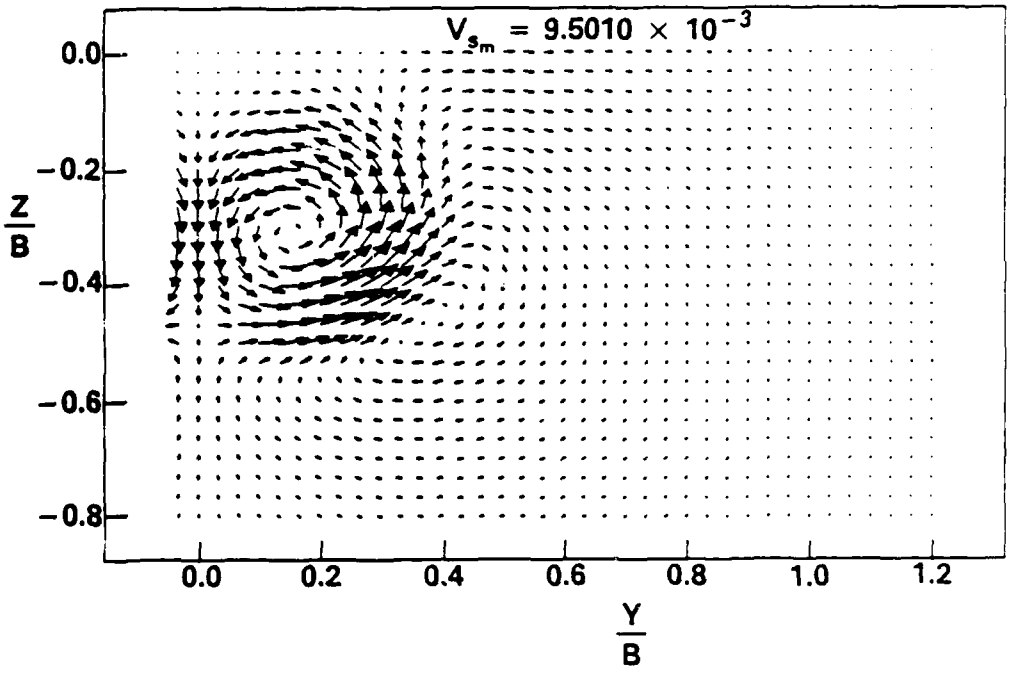

(a) "rigid-lid" surface boundary condition

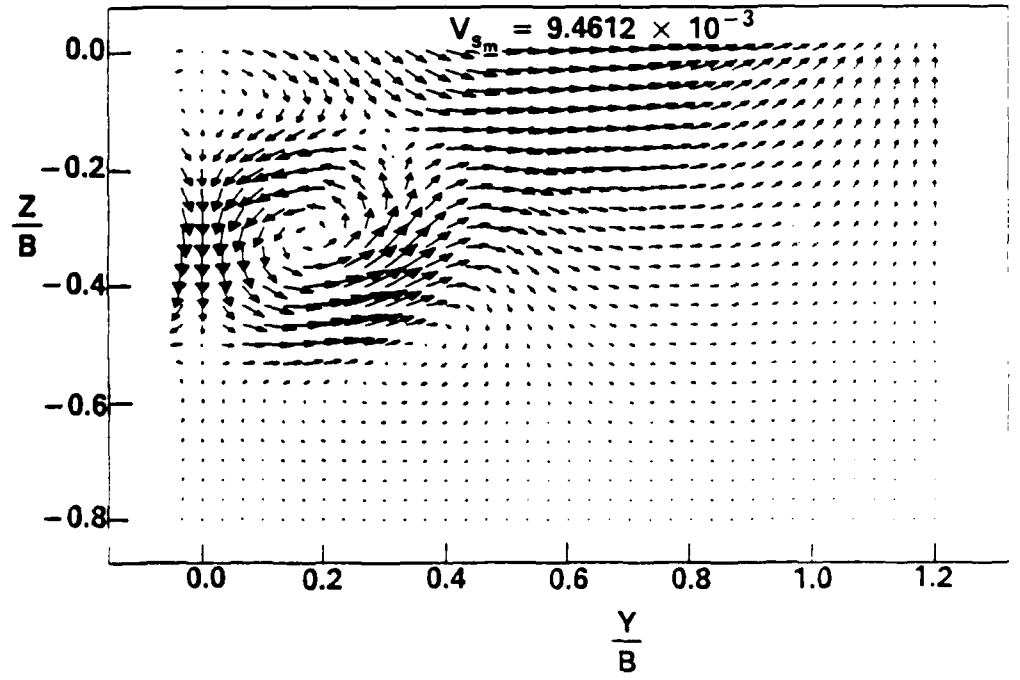

(b) linearized free surface boundary condition

Fig. 9 – Swirl velocity vectors $x = 30.0$ *ft*

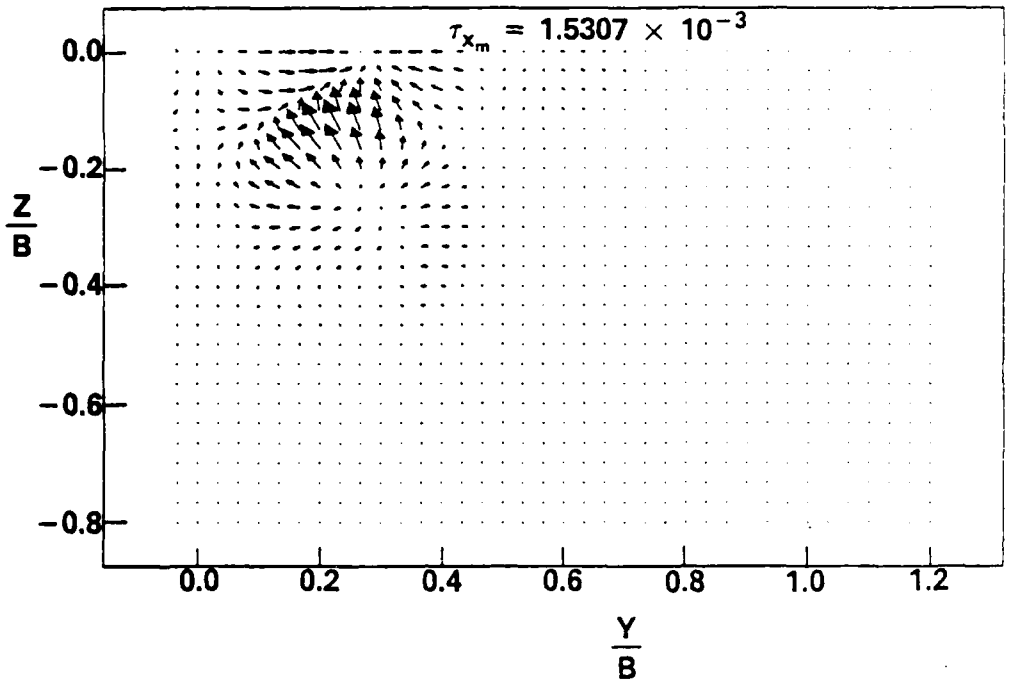

(a) "rigid-lid" surface boundary condition

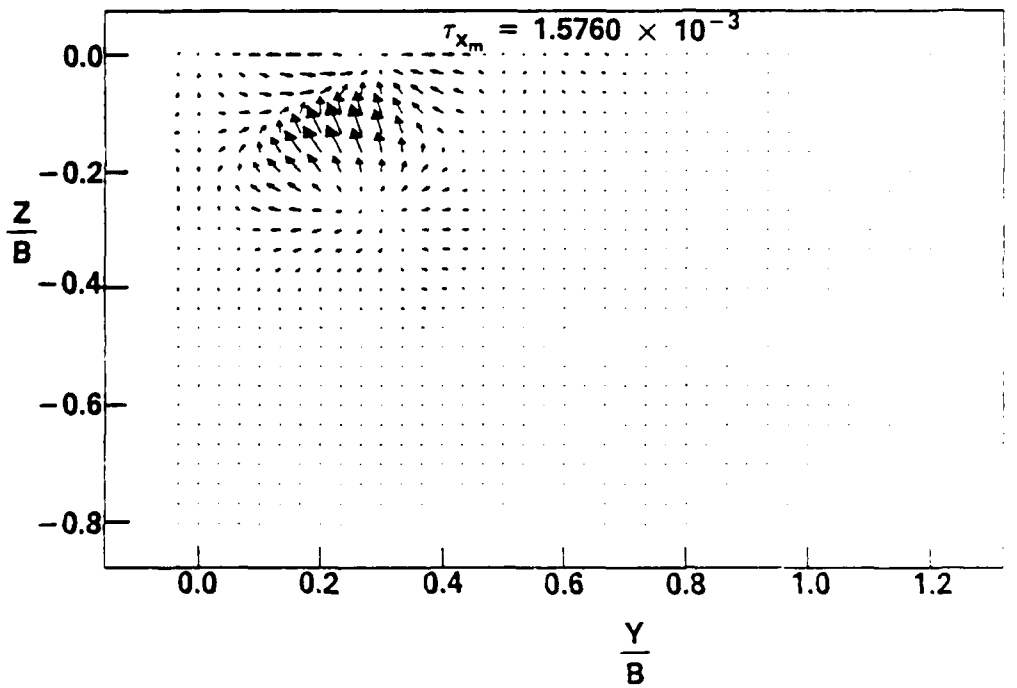

(b) linearized free surface boundary condition

Fig. 10 – Reynolds stress distribution $x = 16.0\ ft$

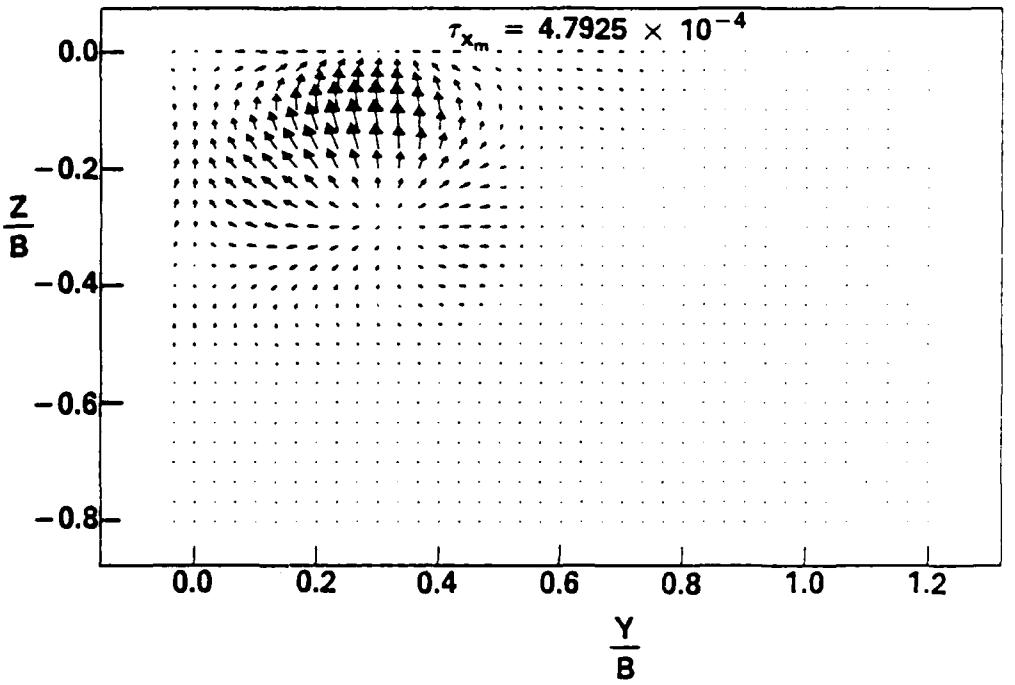

(a) "rigid-lid" surface boundary condition

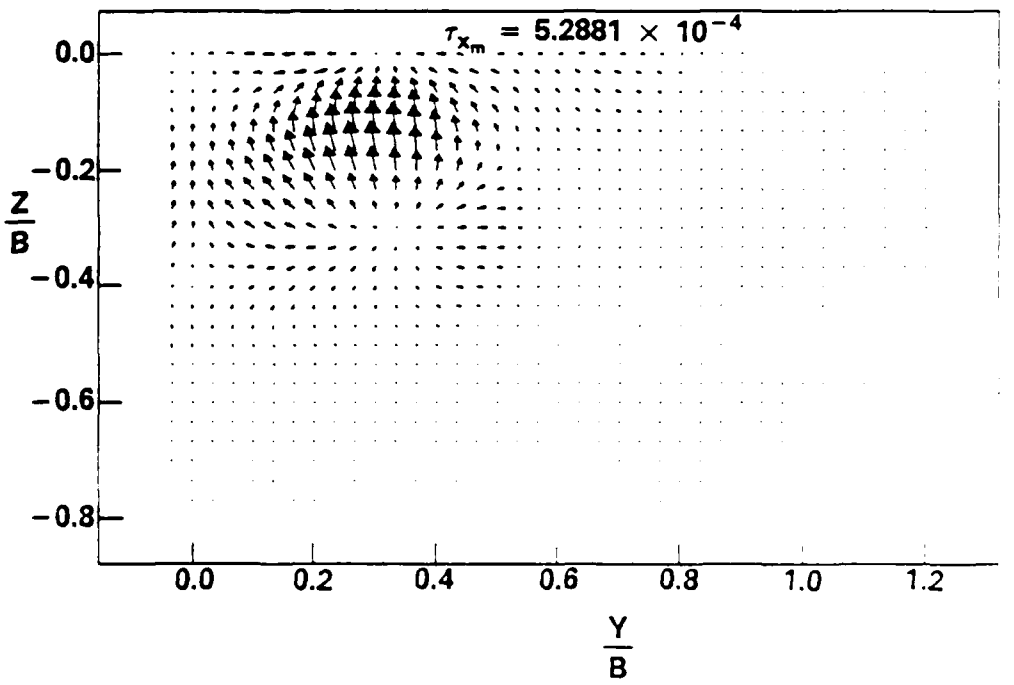

(b) linearized free surface boundary condition

Fig. 11 – Reynolds stress distribution $x = 30.0$ *ft*

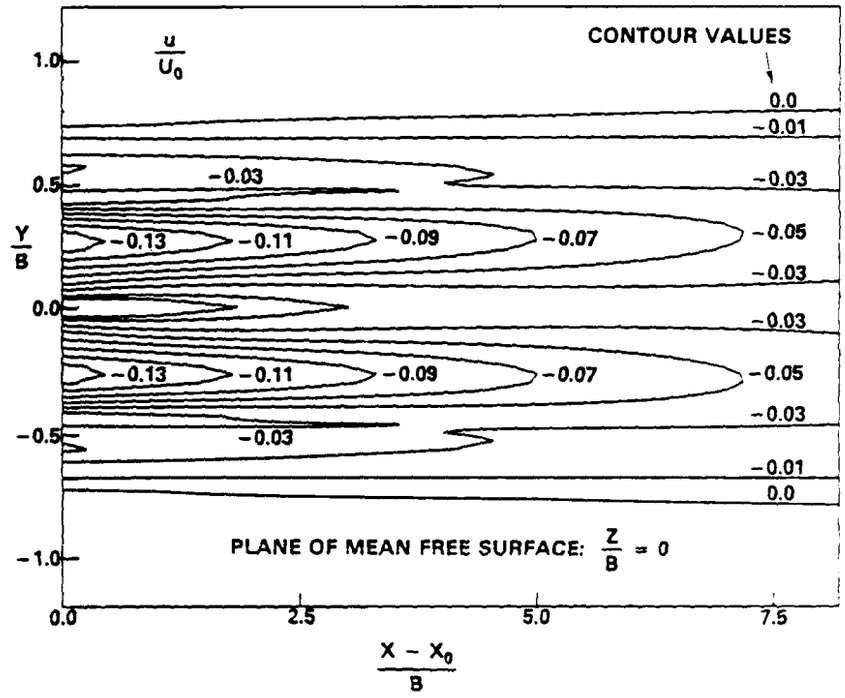

(a) "rigid-lid" surface boundary condition

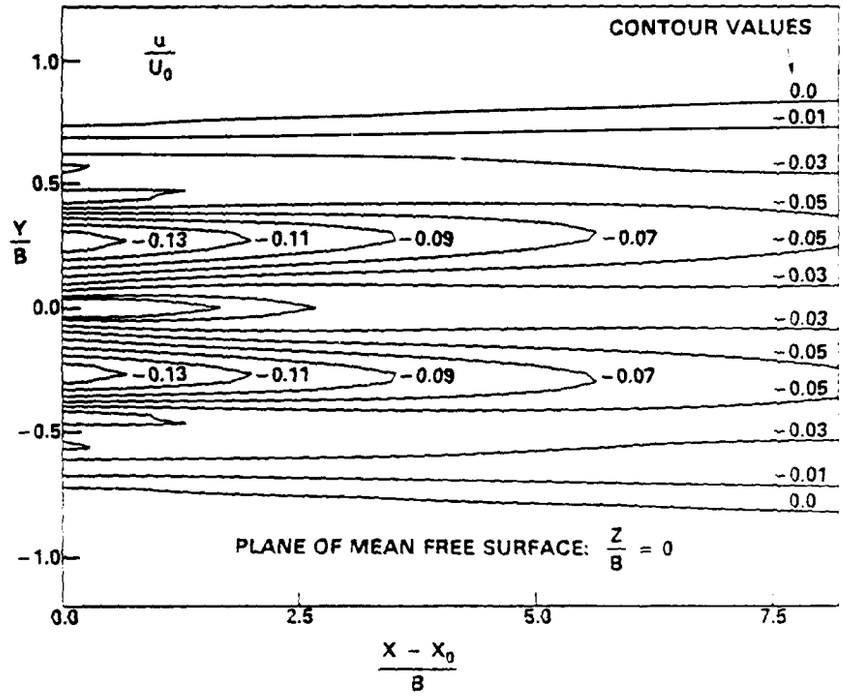

(b) linearized free surface boundary condition

Fig. 12 – Contours of streamwise velocity in plane of free surface

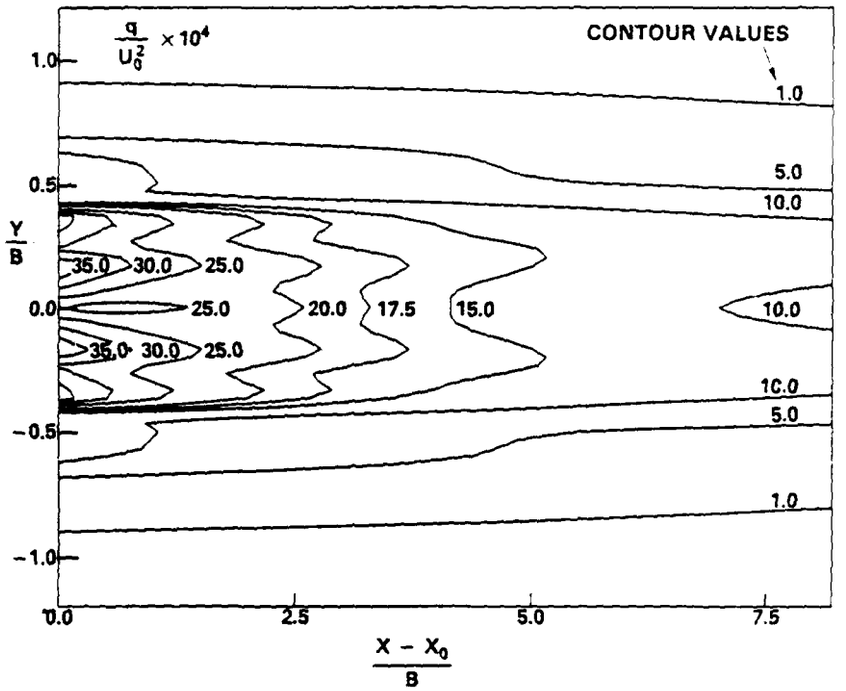

(a) "rigid-lid" surface boundary condition

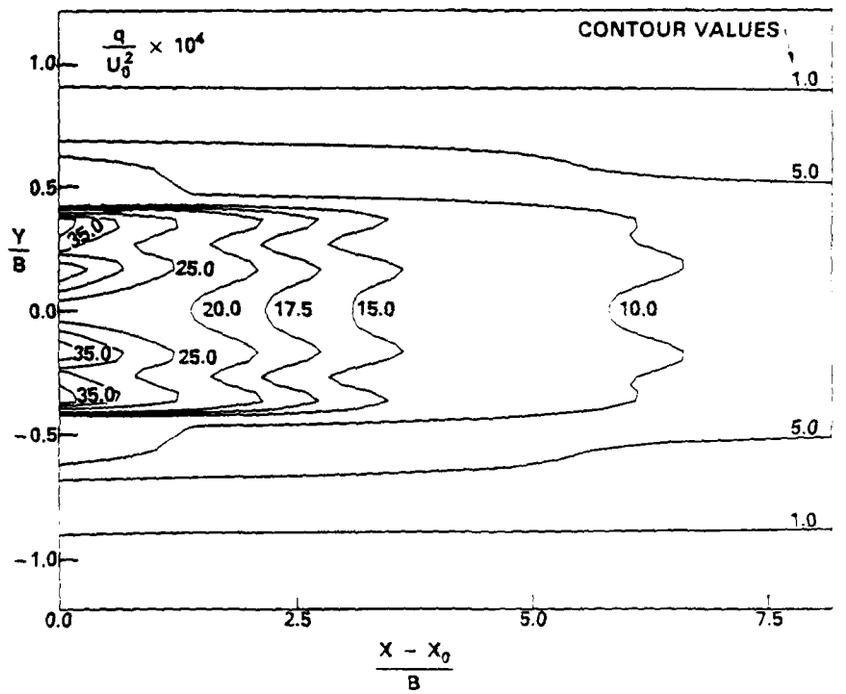

(b) linearized free surface boundary condition

Fig. 13 – Contours of turbulence kinetic energy in plane of free surface

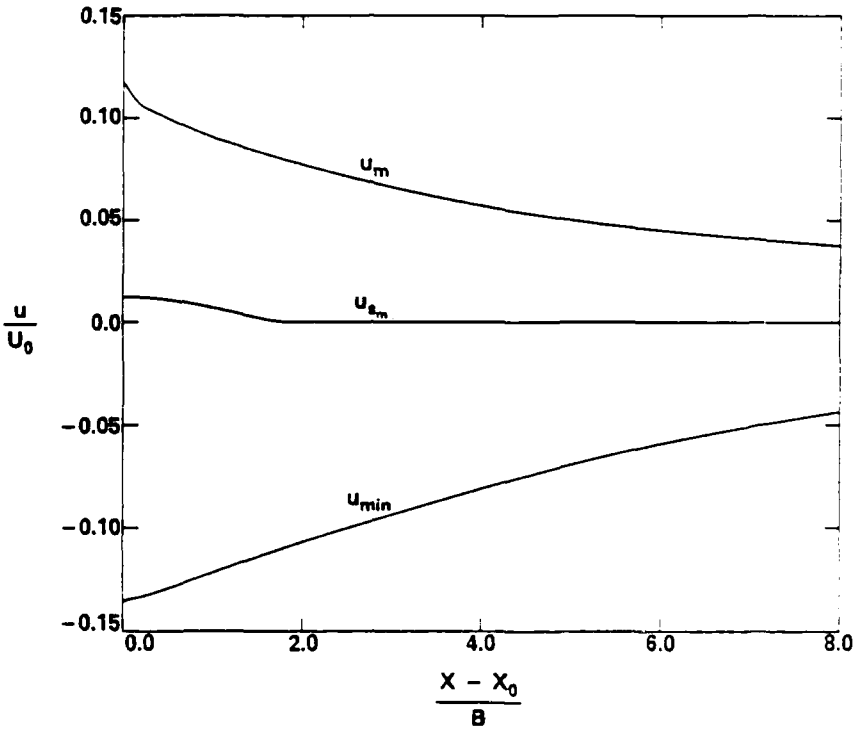

(a) "rigid-lid" surface boundary condition

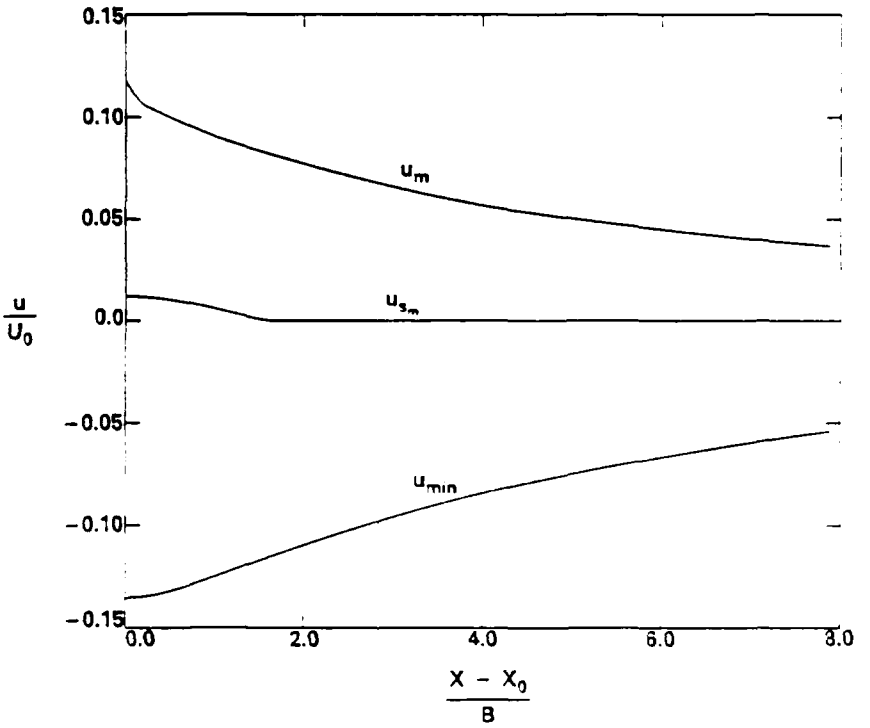

(b) linearized free surface boundary condition

Fig. 14 – Axial decay of characteristic values of streamwise velocity

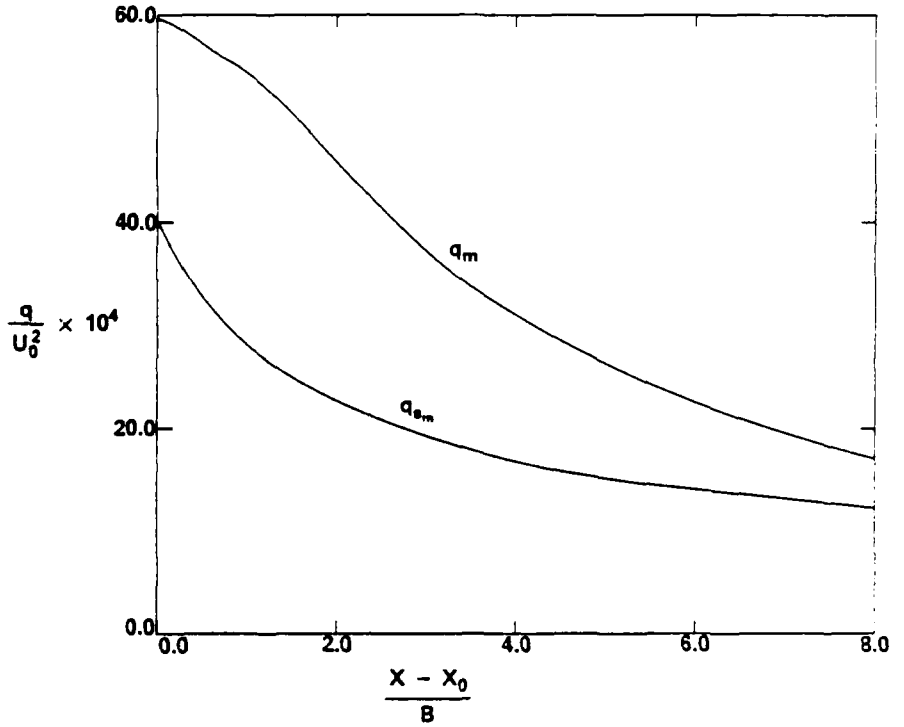

(a) "rigid-lid" surface boundary condition

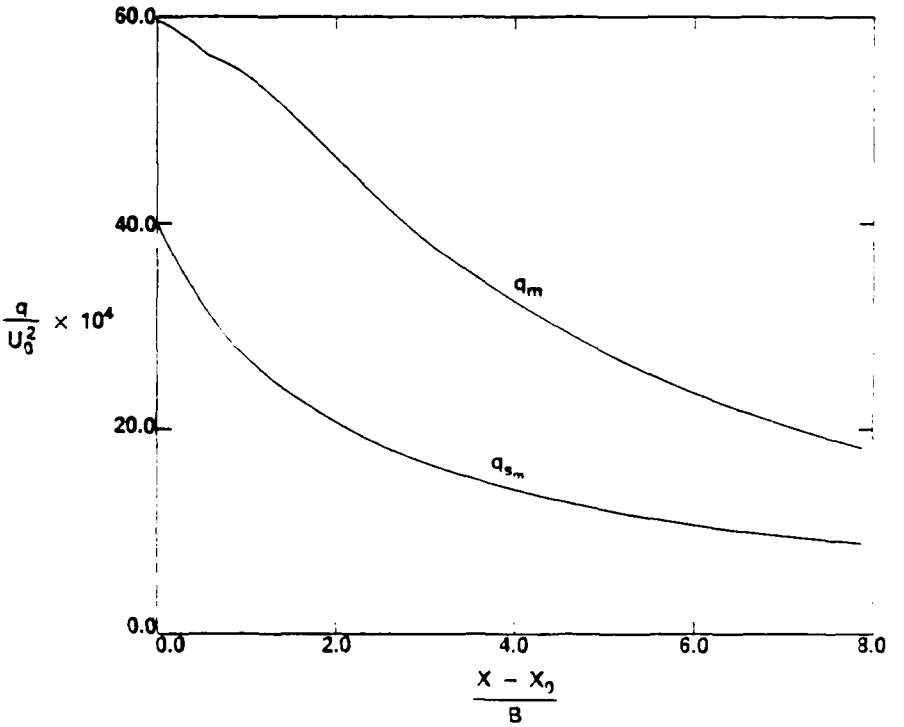

(b) linearized free surface boundary condition

Fig. 15 – Axial decay of characteristic values of turbulence kinetic energy

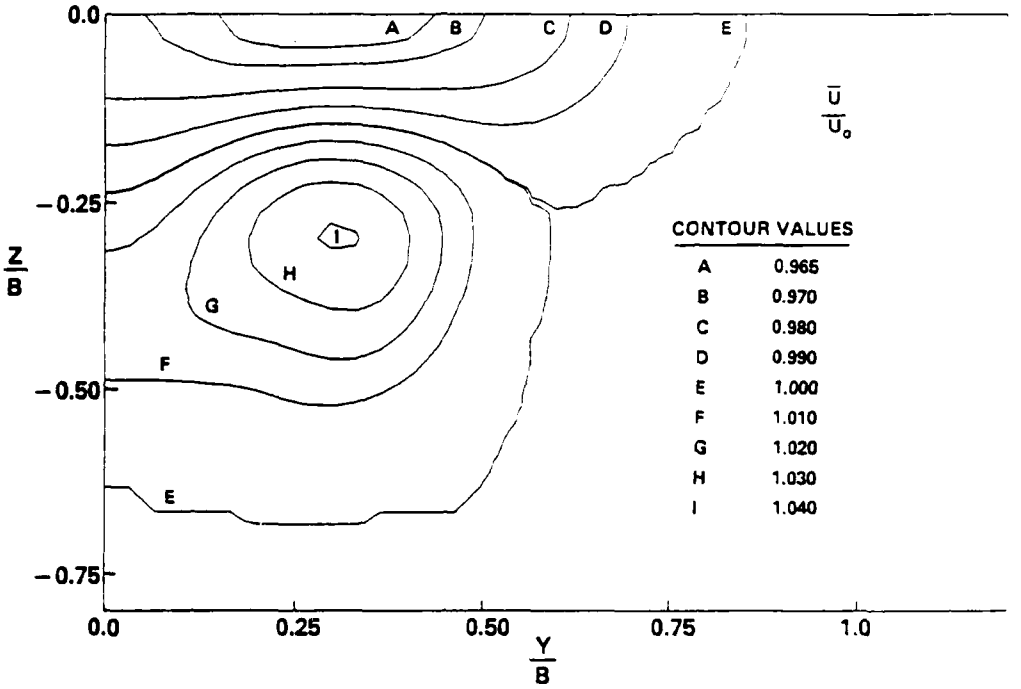

(a) contours of mean streamwise velocity

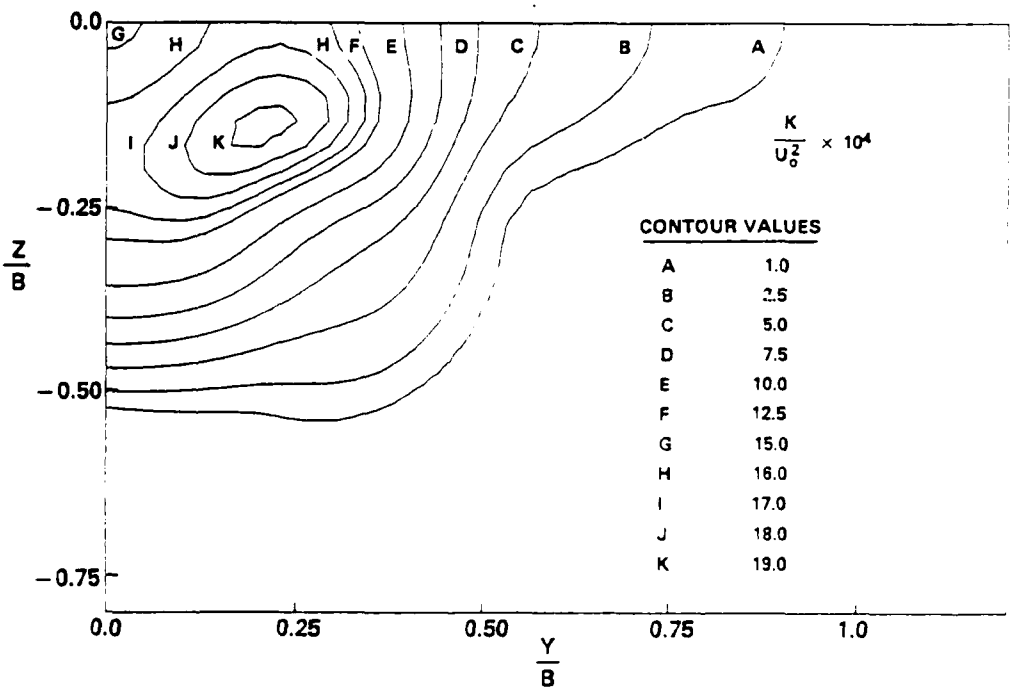

(b) contours of turbulence kinetic energy

Fig. 16 – Distribution of Profile Data from TWAKE simulation [1] – x = 30.0 *ft*

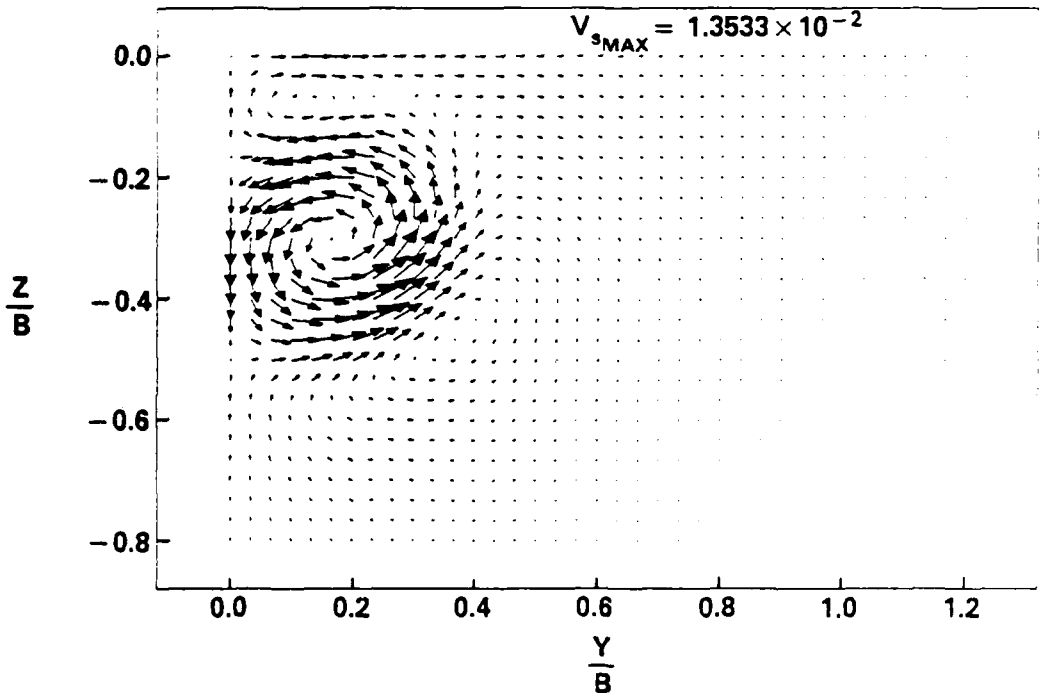

(c) swirl velocity vectors

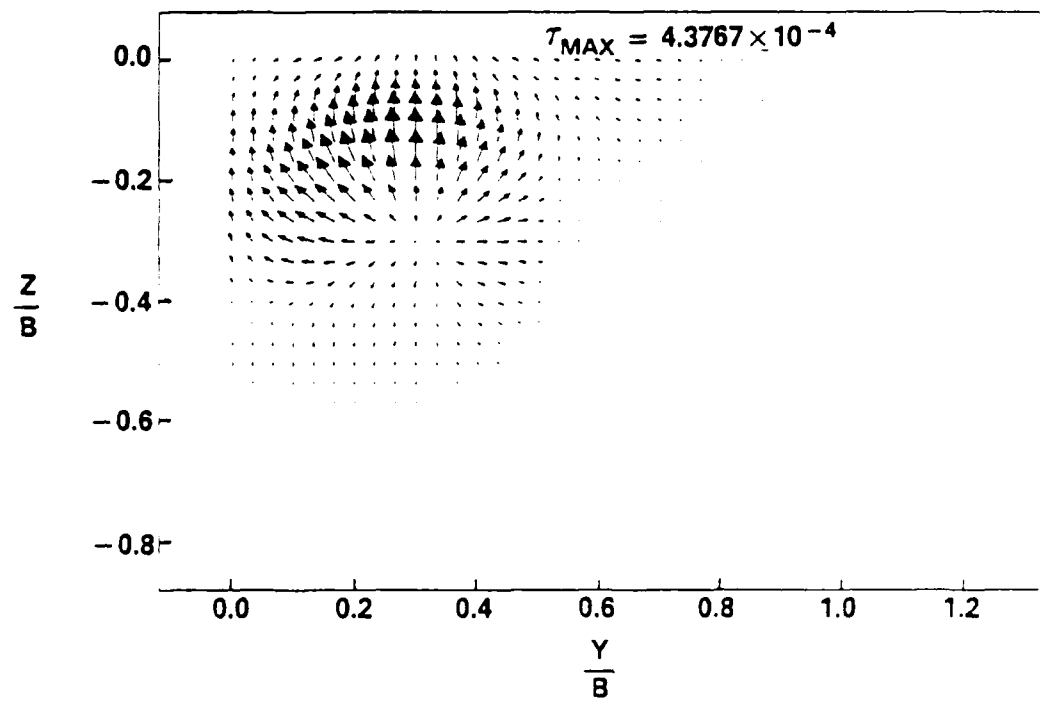

(d) Reynolds stress distribution

Fig. 16 (Cont'd) – Distribution of Profile Data from TWAKE simulation [1] – $t = 30.0$ *ft*

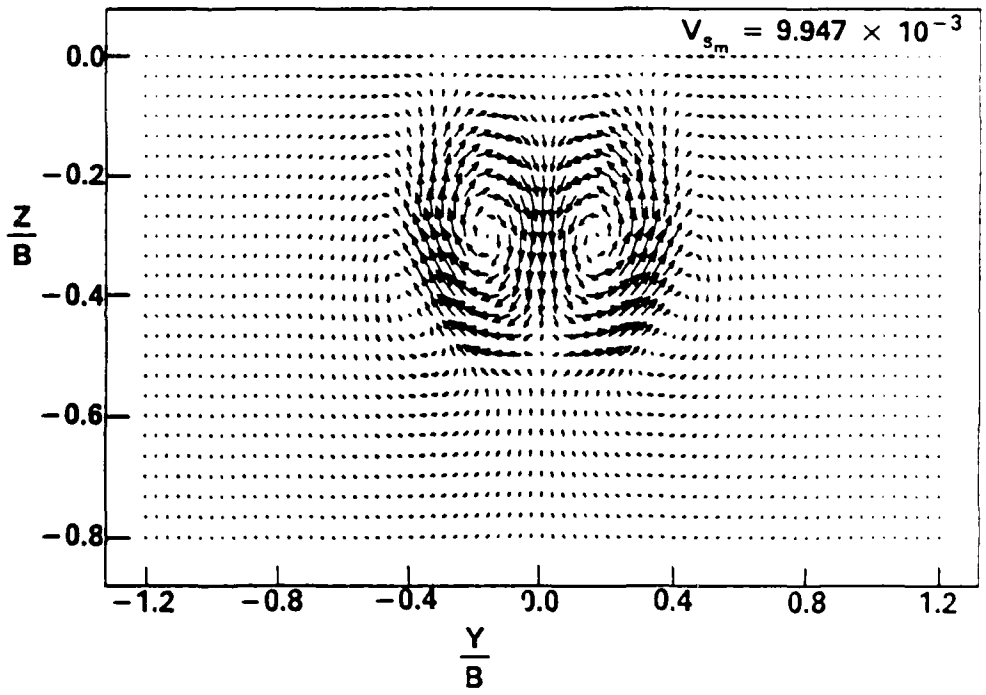

(a) full plane

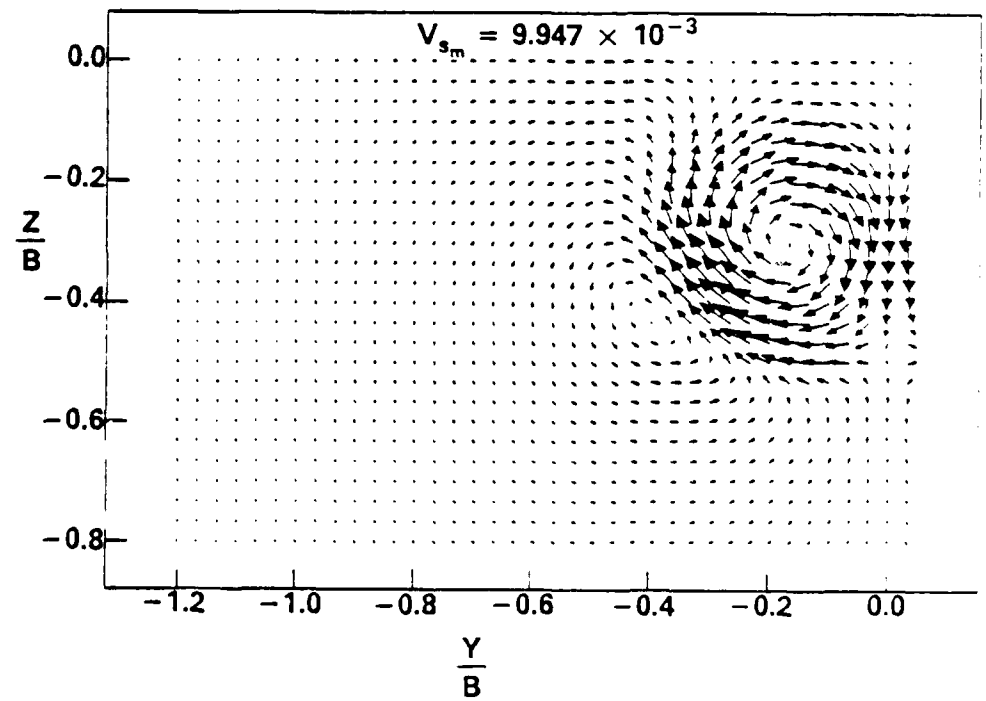

(b) full plane – port half only

Fig. 17 – Swirl velocity vectors; full plane simulation – $x = 30.0$ *ft*

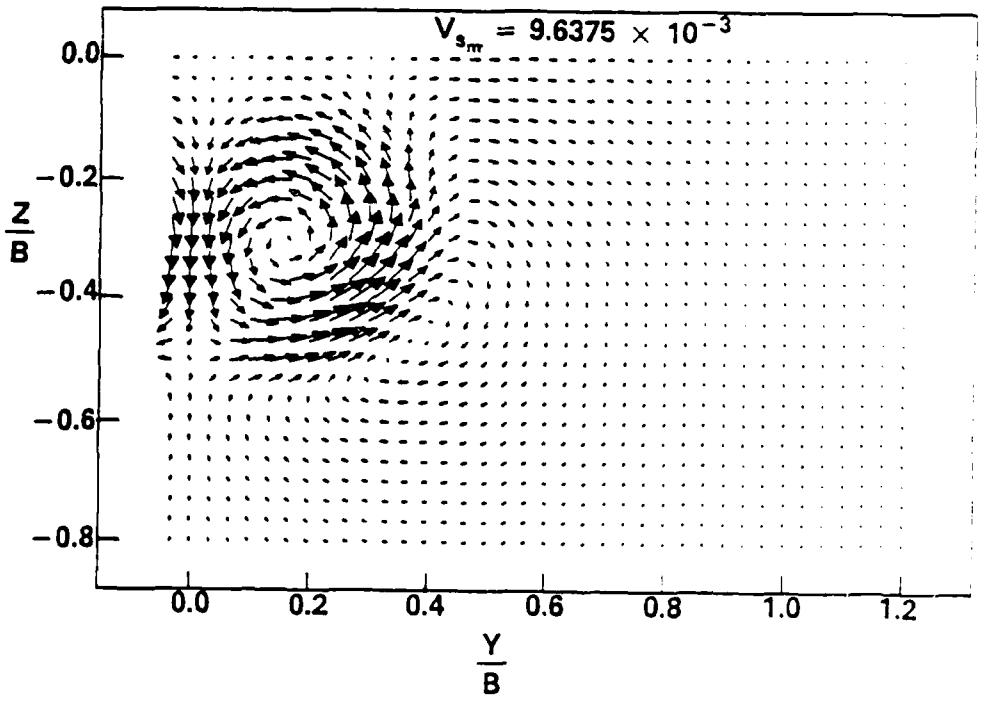

(c) full plane − starboard half only

Fig. 17 (Cont'd) − Swirl velocity vectors; full plane simulation − x = 30.0 *ft*

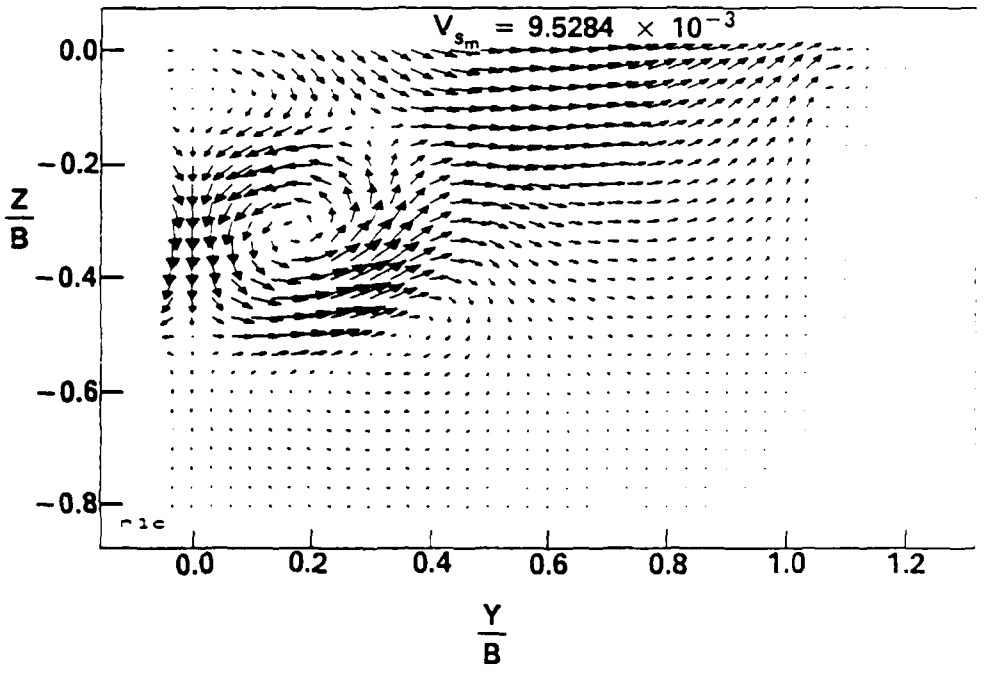

(a) normal width channel

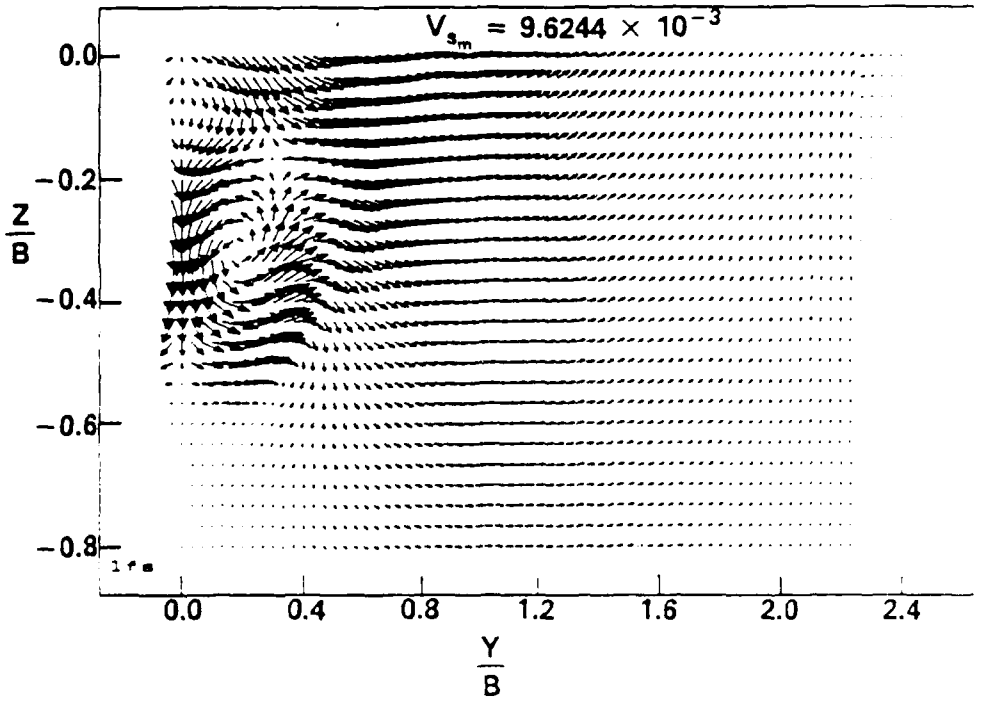

(b) double width channel

Fig. 18 – Swirl velocity vectors; with wave damper – t = 30.0 *ft*

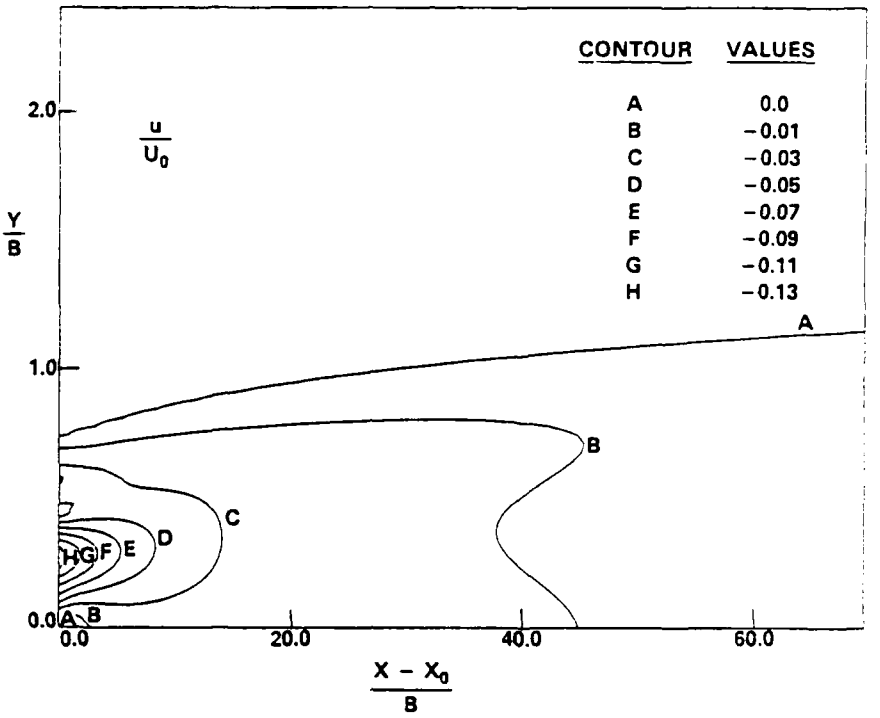

(a) axial velocities (elevations calculated from Eq. (16))

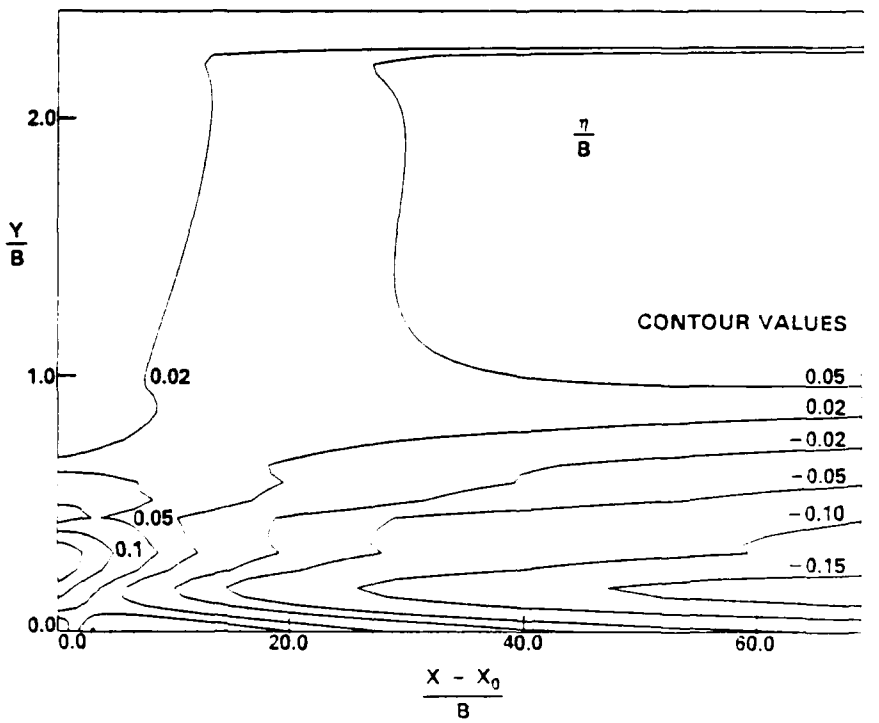

(b) elevations as calculated from Eq. (19)

Fig. 19 – Contours of axial velocity and elevation in plane of free surface